Bed erosion below overflowing weir with an apron

Fang, Siqin.

2010

Fang, S. (2010). Bed Erosion Below Overflowing Weir with an Apron. Final year project report, Nanyang Technological University.

https://hdl.handle.net/10356/91267

BED EROSION BELOW OVERFLOWING WEIR WITH AN APRON

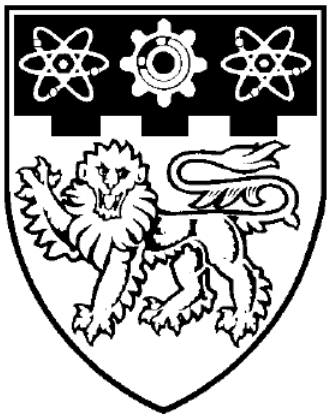

FANG SIQIN

SCHOOL OF CIVIL AND ENVIRONMENTAL ENGINEERING
COLLEGE OF ENGINEERING
NANYANG TECHNOLOGICAL UNIVERSITY

2009

BED EROSION BELOW OVERFLOWING WEIR WITH AN APRON

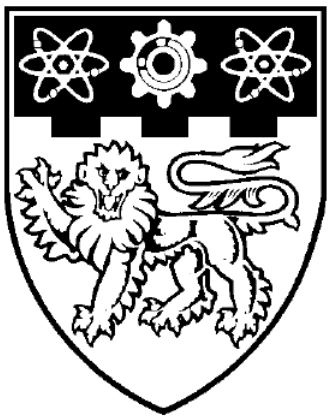

Submitted by
FANG SIQIN

School of Civil and Environmental Engineering
College of Engineering
Nanyang Technological University

A Final Year Project presented to the Nanyang Technological University
in partial fulfillment of the requirements for the
Degree of Bachelor of Engineering

2010

Abstract

The project is conducted to investigate the scouring phenomenon at the downstream of an overflowing weir with and without an apron. Apart from studying the changes in the general bed scour profile, the equilibrium scour condition is the key focus.

This is achieved by reviewing the concepts that were critical to the study. Following which, the study was completed by conducting 28 experiments on a 8.0m long by 0.3m wide by 0.6m deep flume where the scour profiles were being periodically recorded during the experiment. Nevertheless, the experiments were conducted by focusing on the effect of varying flowrate, water depth differences and apron length; other parameters were left constant.

The results show that the formation of scour hole is dependent on the three mentioned parameters whereas the increase in flowrate, increase in water depth differences and decrease in apron length will all lead to an increase in the scour depth. Empirical correlations were established to predict the equilibrium scour time, equilibrium maximum scour depth and scour-time development with flowrate and water depth differences. The accuracy of the prediction is as high as 80% of the actual depth which is deemed to be within the satisfaction limit. It was found that the apron must have a minimum length so that the plunging nappe will not strike the erodible bed. In addition, the scour depth can be reduced by almost 80% when the apron length to water depth above the weir crest ratio approaches a certain magnitude.

Acknowledgements

The author would like to acknowledge and extent his heartfelt gratitude to Dr. Lim Siow Yong, Project Supervisor, for his invaluable advice and professional guidance throughout the project who has made the completion of his project a success. In addition, the author would also like to express his thanks to Mr. Lim Kok Hin, Mr. Foo Shiang Kim, Mr. Chia Key Huat, Mr. Fok Yew Seng and Mr. Syed Alwi Bin Sheikh Bin Hussien Alkaff for providing the necessary laboratory support and assistance while conducting the experiments.

Table of Contents

List of Appendices

List of Tables

List of Figures

List of Symbols

B	*Width of Channel*	h	*Water Depth above Crest of Weir*
C_d	*Discharge Coefficient*	h_1	*Water Depth at Upstream of Weir*
c_s	*Coefficient with Dimension, 4.75*	h_2	*Tailwater Depth*
d	*Scour Dimension in Vertical Direction*	k_W	*Weir Discharge Coefficient*
$d_{15.9}$	*Grain Size corresponding to 15.9% Finer by Dry Weight*	L	*Scour Dimension in Horizontal Direction*
d_{50}	*Grain Size corresponding to 50% Finer by Dry Weight*	$L`_p$	*Length at Maximum Deposition Height*
$d_{84.1}$	*Grain Size corresponding to 84.1% Finer by Dry Weight*	$L`_{pe}$	*Length at Equilibrium Deposition Height*
d_{90}	*Grain Size corresponding to 90% Finer by Dry Weight*	$L`_s$	*Length at Maximum Scour Depth*
d_b	*Scour Depth at Brink*	$L`_{se}$	*Length at Equilibrium Maximum Scour Depth*
d_{be}	*Equilibrium Scour Depth at Brink*	L_p	*Length at End of Deposition*
d_p	*Deposition Height*	L_{pe}	*Length at End of Deposition at Equilibrium*
d_{pe}	*Equilibrium Deposition Height*	L_s	*Scour Length*
d_s	*Maximum Scour Depth*	L_{se}	*Equilibrium Scour Length*
d_{se}	*Equilibrium Maximum Scour Depth*	L_W	*Width of Weir*
d_{sf}	*Maximum Scour Depth corresponding to End of Experiment*	P	*Height of Weir*
Fr	*Froude Number,* $\frac{u}{\sqrt{gh}}$	Q	*Discharge*
Fr_d	*Densimetric Froude Number,* $\frac{u}{\sqrt{(S-1)gd_{50}}}$	q	*Discharge per unit Width,* $\frac{Q}{B}$
g	*Gravitational Acceleration,* $9.81 m/s^2$	Re	*Reynolds Number*

Re^*	*Boundary Reynolds Number*
S	*Specific Gravity of Sediment,* $\frac{\rho_s}{\rho}$
t	*Time*
t_e	*Equilibrium Scour Time*
u	*Mean Velocity across Weir,* $\frac{Q}{hB}$
x	*Length of Apron*
Δh	*Water Depth Difference,* $h_1 - h_2$
θ_c	*Critical Shear Stress*
μ	*Dynamic Viscosity of Water,* 10^{-3}*kg/m·s*
ρ	*Density of Water, 1000kg/m*^{3}
ρ_s	*Density of Sediment, 2650kg/m*^{3}
σ_g	*Geometric Standard Deviation,* $\sqrt{\frac{d_{84.1}}{d_{15.9}}}$

1 Project Introduction

1.1 Purpose

The main objective of this project is to conduct a quantitative analysis on the equilibrium scour condition at the downstream of an overflowing weir. The influence of flowrate and tailwater depth on the scouring phenomenon will be the main focus in this study. Apart from equilibrium condition, a model to predict the temporal change in the maximum scour depth will be established. In addition, a preliminary investigation was also carried out to understand the impacts of apron on the equilibrium maximum scour depth.

1.2 Background of Studies

As mentioned in Akan (2006), weir is a hydraulic structure that is mounted perpendicular to the flow direction in rivers or streams. In order for the river to flow downstream, the water level has to build up at the upstream until it is able to overflow from the weir. Thus, the overflowing water behaves like an impinging jet, also known as nappe flow, and strikes the tailwater at the downstream side which will create disturbances to the flow.

If the downstream bed is alluvial and unprotected, scour will form instantaneously if the jet has sufficient energy to penetrate the bed. Scouring is a fluvial process where a hole is formed on an erodible bed due to the transport of sediments by hydraulic movement. This phenomenon can be commonly detected near places where hydraulic structures are erected. Annandale (2006) reported that there is 30m deep granite scour hole developed at the downstream of the Arizona's Bartlett Dam. There is also similar problem encountered at the Kariba Dam in Africa where the scouring effect caused a formation of a 80m deep plunge pool which is close to two-third of the dam's height. Excessive scouring on the bed is undesirable as it poses a threat to the stability of the structure's foundation. Therefore, in order to determine the pilling depth, designers are interested to acquire the details of the equilibrium scour condition; especially the equilibrium maximum scour depth.

Nevertheless, there are instances whereby the postulated equilibrium maximum scour depth is too large and unacceptable, Hoffmans and Verheif (1997) highlighted that the immediate downstream of a weir can be engineered with protection to minimize it. Concrete apron is a bed protecting structure that is installed at the downstream of the hydraulic structure whenever there is an abrupt change in the flow condition. The presence of an apron will provide time and space for the turbulence flow to decay before it reaches the erodible bed. Since apron is an engineered

structure, therefore it will not be cost effective to design and construct long stretches of protection as it requires plenty of time and space for the flow to dissipate its scouring energy. Hence, investigations have to be carried out in order to have better understanding in the equilibrium scour condition and the effect of the apron length on scour hole formation.

1.3 Scope

The followings are included in this report:

- Review the critical concepts that will facilitate the study
- Provide an outline of experimental set-up and procedures
- Describe the parameters affecting the scour profile
- Determine the normalized scour-time relationship
- Predict and verify the scour-time development relationship
- Correlate the effects of apron length to equilibrium scour depth
- Provide suitable recommendations for future studies

2 Literature Review

This Chapter aims to provide a review of the background knowledge that is useful for this study. In addition to the critical concepts, some of the related studies and useful analysis tools will also be elaborated in this segment.

2.1 Overflowing Weir

Types of Weir

A weir is a flow measurement device that is normally mounted perpendicular to the flow direction in rivers or streams. According to Jain (2001), weirs can be divided into the following categories (See Figure 2-1 to Figure 2-4):

- Form of opening

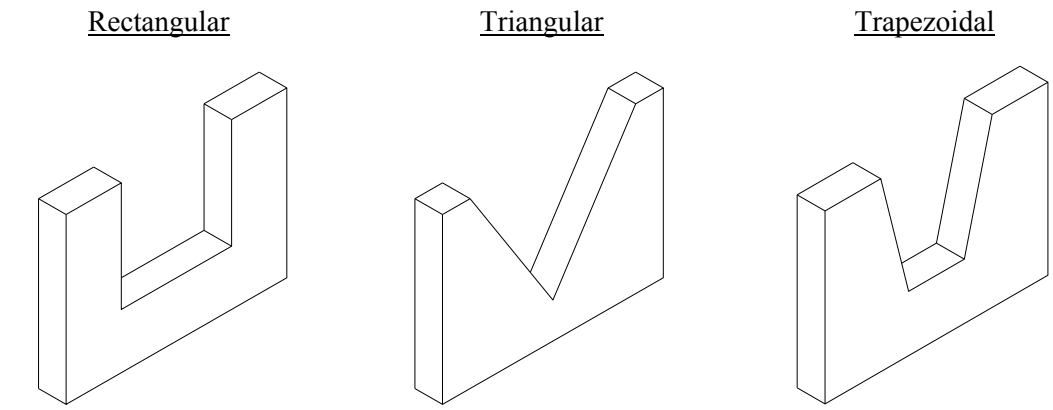

Figure 2-1: Form of Opening

- Types of Edge

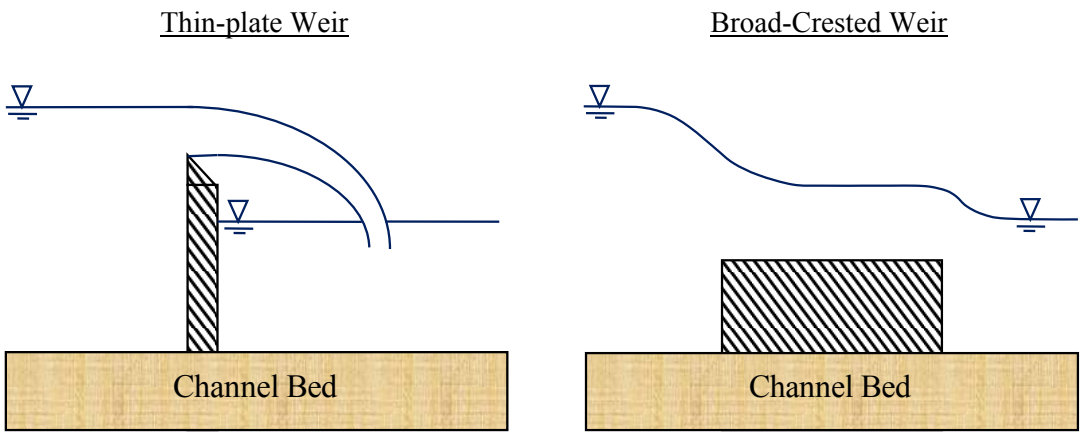

Figure 2-2: Types of Edge

- Discharge Condition

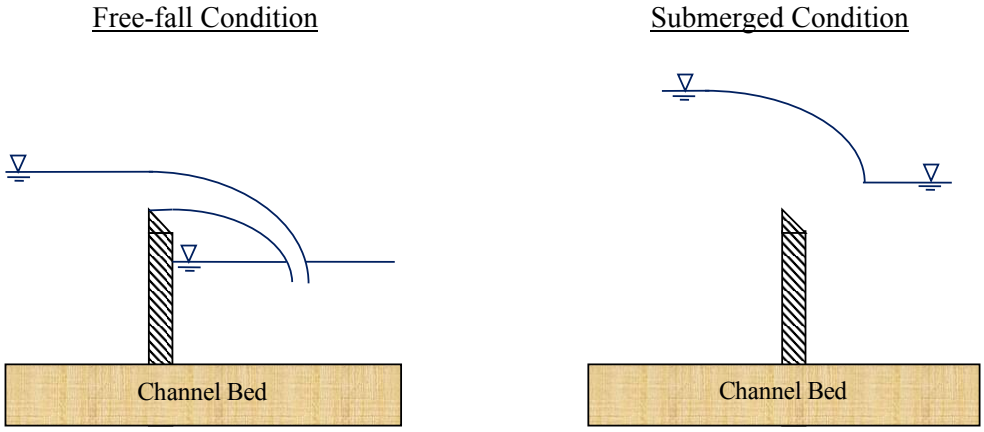

Figure 2-3: Discharge Condition

- Ends Condition

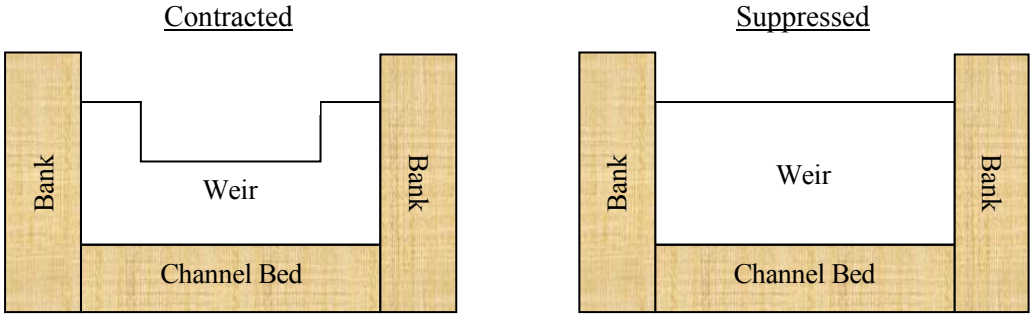

Figure 2-4: Ends Condition

Weir Discharge

Many studies have been conducted to propose discharge equations for different types of weir; the discharge is usually correlated to the flow depth above the crest, *h* of the weir (See Figure 2-5*)*.

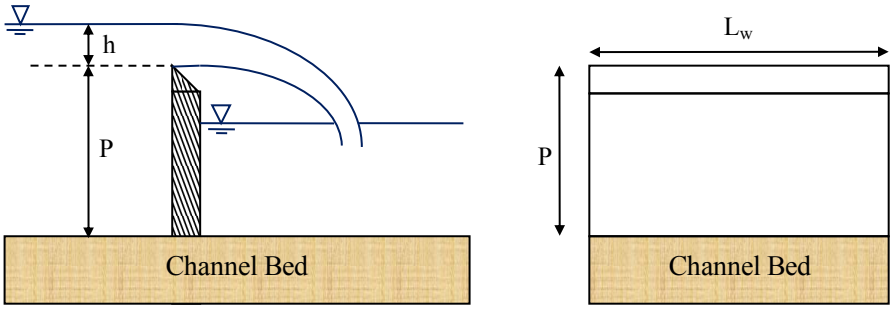

Figure 2-5: Side & Cross-sectional View of Thin-plate Weir

One of the common discharge equations is given as Akan (2006),

$$Q = \frac{2}{3} C_d \sqrt{2g} L_w h^{1.5} \quad (2\text{-}1)$$

Where Q, discharge across the weir (m^3/s) C_d, discharge coefficient; L_W, width of weir (m) and h, height of water above crest (m). Equation (2-1) can be rewritten by introducing the weir discharge coefficient, $k_w = \frac{2}{3} C_d$, and it can be simplified to:

$$Q = k_w \sqrt{2g} L_w h^{1.5} \quad (2\text{-}2)$$

The weir discharge coefficient can be obtained from Figure 2-6 by using ratio of $\frac{h}{P}$ and $\frac{L_w}{B}$; where B and P represents the width of channel and height of weir respectively.

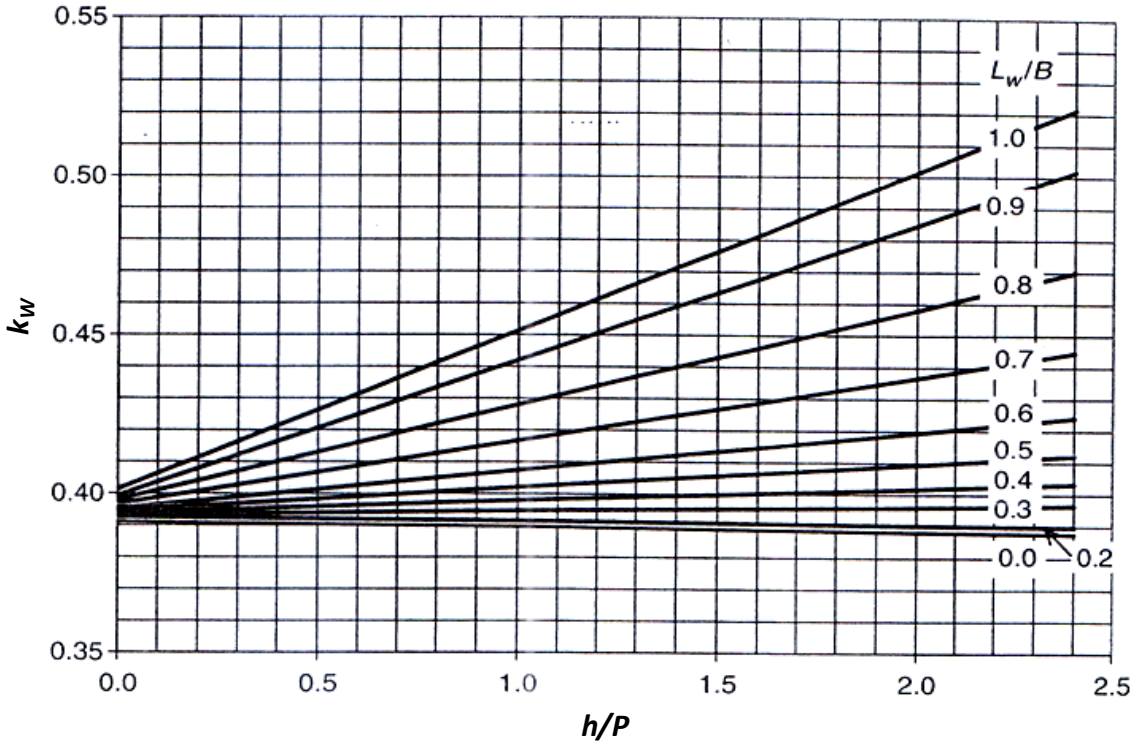

Figure 2-6: Weir Coefficient Graph

As soon as the water accumulates and overflow from the weir, in the context of thin plate weir, the water will spring out and behave like an impinging blade which will create massive disturbance to the downstream flow which is shown in Figure 2-7 that is reported in Akan (2006). The springing of water over the weir is known as nappe. Similar phenomenon can also be observed at the overflow weir that are used to dam reservoir as shown in Figure 2-8.

Figure 2-7: Luscombe Weir, Queensland, Australia

Figure 2-8: Marina Barrage, Singapore

2.2 Sediment Transport

Initiation of Motion

The initiation of motion of particles indicates when the water flow has sufficient energy to cause the grain to move randomly on the sediment bed. Such movement is dependent on a range of factor such as the fluid density, kinematic viscosity, sediment density and grain size. Therefore, due to the variation in shapes and sizes, individual grain will have different dimensionless critical shear stresses, θ_c in order to initiate their motion; thus the critical shear stress of particles adopts a probability distribution.

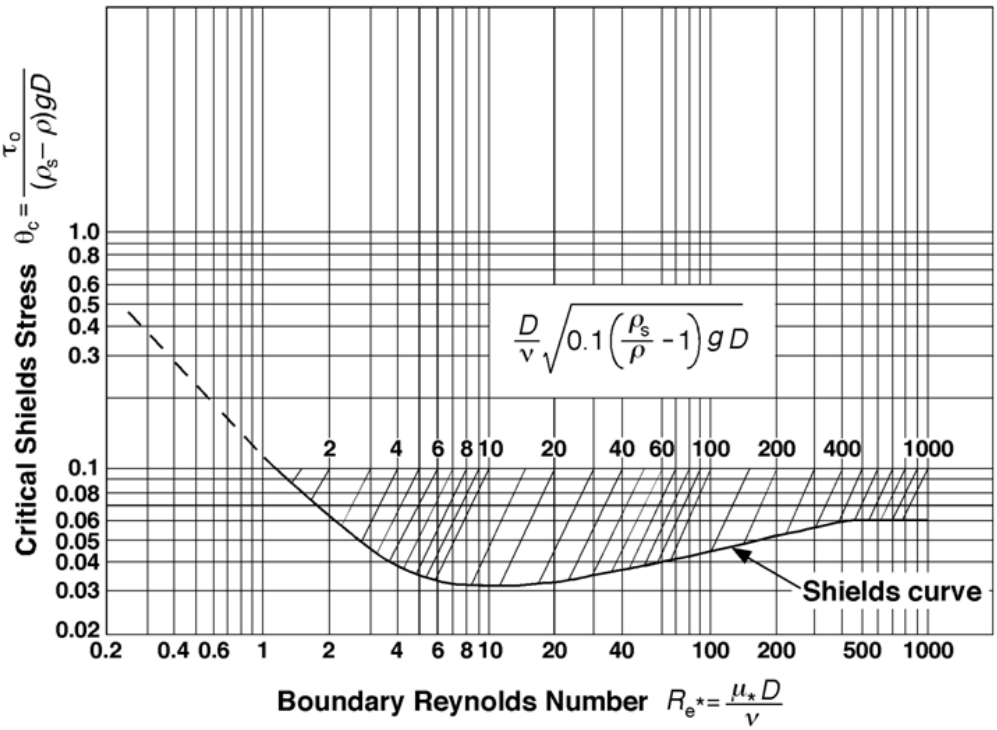

Figure 2-9: Shields Diagram

Shields had published his concept for the initiation of movement of uniform granular particles on a flat bed. Figure 2-9 in the previous page shows the Shields Curve which gives the averaged critical value of the shear stress.

According to Chien and Wan (1999), the curve suggests that at a Boundary Reynolds Number, $Re*$ of approximately 10, the critical shear stress is at its minimum. In addition, when the $Re*$ is smaller than 2, Shields proposed a linear relationship between θ_c and velocity where the incipient motion is independent of the grain size. On the contrary, when $Re*$ is greater than 10, θ_c will increase as the grain size increases. If the $Re*$ approaches 1000, θ_c will have a rough constant value of 0.06.

Bed-load Transport and Suspended-load Transport

As soon as the sediment's shear stress increases beyond the critical limit, the particles will be transported by two modes of transport: bed-load or suspended load. The basic form of bed-load consists of rolling, sliding and saltation. Saltation occurs when the grains are transported in a series of irregular jumps and bounces along the erodible bed. On the other hand, suspended-load describes the transportation of sediments whereby particles are being entrained by the fluid and carried downstream (See Figure 2-10).

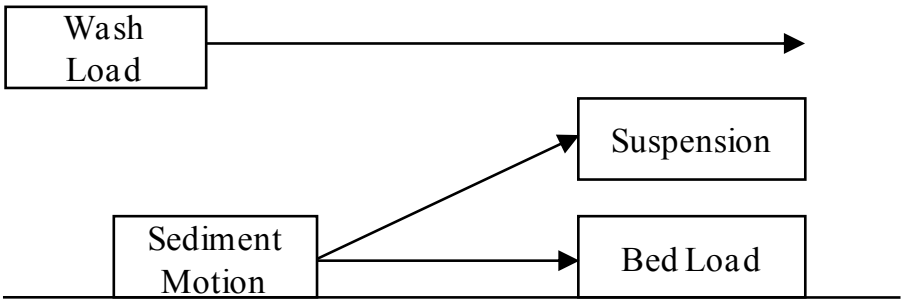

Figure 2-10: Schematic Diagram for Transportation of Sediment Load

Sediment suspension often occurs when the flow is highly turbulent such that it has sufficient energy to balance the particle weight. The transport of suspension is normally stimulated by turbulent diffusion and convection. The diffusive transport is characterized by the random motion through the bulk flow direction. Since the sediment concentration is usually larger at the bed, the longitudinal flow will generate an ascendant migration of grain to the region of lower concentrations. Whereas for convective transport, particles are being mobilized by large vortices in which they will remain afloat while transported downstream. When sediments are being suspended and do not interact with the channel bed during the transportation, they can be termed as wash load.

2.3 Scouring

As mentioned earlier, nappe that overflow from the weir will create turbulence to the downstream flow. If the downstream of the weir consists of a non-static bed, the impinging jet flow will induce hydraulic movement which will then induce sediment transport or erosion. Erosion that is caused by man-made obstacles is commonly known as scouring.

General Scour and Local Scour

There are different forms of scour; general or local. General scour will occur along the river when there is constriction, bend or confluence (branches of river meet at an angle) where local scour occurs when the flow is being disrupted by hydraulic structures. Some of the structures include bridge piers, abutments and weirs. Hoffmans and Verheif (1997) reported that the time scale is the main difference to differentiate these two main groups of scouring.

Time scale for scouring is defined as the time interval to develop a substantial scour. Basically, the presence of obstruction along the water flow will create local eddies around the structures, and if the energy from these eddies is able to initiate the motion of the erodible bed, scouring will occur. The presence of hydraulic structures will induce a higher degree of local destructive turbulence as compared to the change in channel geometry; such occurrence will therefore enhance the formation of scour. Hence, local scouring typically has a shorter time scale as compared to general scouring.

Clear-water Scour and Live-bed Scour

As discussed in the earlier paragraphs, scours will be created by hydraulic movement that is being caused by interferences along the channel. However, the scale of scouring is affected by the types of hydraulic movement which are known as the clear-water and live-bed scour. Clear-water scour simply implies that the flow that causes scour does not contain any upstream sediment transport while live-bed scour depicts otherwise. As a result, this indicates that the live-bed scour will probably has a smaller maximum scour depth when compared to the clear-water scour as the upstream sediments will be deposited at the hole in the midst of live-bed scouring.

Evolution in Clear-water Scour

According to Hoffmans and Verheif (1997), the evolution of scour hole under clear-water scouring can be distinguished into four phases; namely the initial phase, development phase, stabilization phase and an equilibrium phase.

The rate of erosion is the most rapid during the initial phase where particles will be dispersed in random direction. However, most of the particles will be suspended and transported longitudinally downstream and some will be carried as bed load which follows the convectional flow path. As soon as the development phase sets in, there is a significant decrease in the amount of suspended load. Nonetheless, the scour size increases tremendously during this stage but the ratio between the scour length and scour depth remains unchanged. During the stabilization phase, the overall rate of scouring decreases. The scouring capacity begins to retard at the maximum depth while the erosion capacity maintain at the downstream of the scour hole; this causes the greater increment in the scour length than its depth. Eventually, when the dimensions of the scour hole do not change significantly, the scour is slowly approaching the equilibrium phase.

Scour at Hydraulics Structure

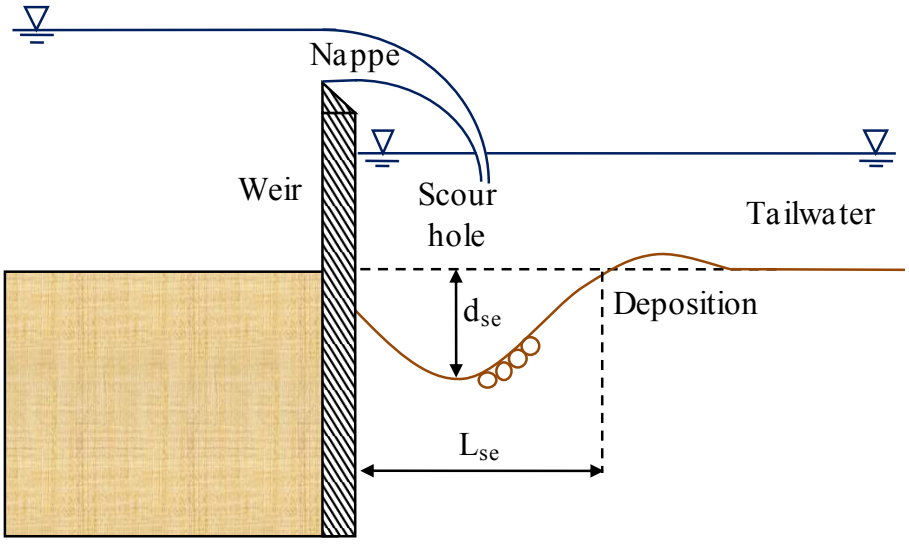

Figure 2-11: Schematic Diagram of Scouring at Downstream of Weir

Scour at the hydraulic structure is categorized as one of the local scour as shown in Figure 2-11. The bed will be eroded instantaneously if the downstream of the weir is left unprotected. The scour development is a dynamic process that is considerably complicated to analyze it quantitatively. Therefore, the emphasis is generally being placed on the equilibrium maximum scour depth, d_{se} and length, L_{se} which it is the dimension of the scour hole at the equilibrium phase.

2.4 Scour Protection

Protection Options

Scouring is an undesirable phenomenon in waterways as it will threaten the stability of the hydraulic structure. Therefore, there must be measures to minimize the scouring effect. A review by Annandale (2006) listed the followings six feasible approaches that can be employed for scour protection:

- *Flow Boundary Pre-forming* – Construct a predicted maximum scour hole so as to reduce the erosive capacity.
- *Accommodating Protection* – Construct adjacent infrastructures in manner which are not within the boundaries of the predicted scour.
- *Earth Material Enhancement* – Enhance resistance to erosion through planting vegetation and rock anchorage.
- *Hard Protection* – Use riprap, concrete or other lining systems to protect the earth from erosion.
- *Flow Modification* – Alter the flow condition whereby its turbulence is being reduced to a less significant level.
- *Combination* – Optimize the protection by incorporating different protection system together.

Hard Protection

This method entails the use of materials to fortify the predicted scour area. Within this approach, one of the techniques is to design riprap (See Figure 2-12). This involves the placement of rocks in ways that the underlying erodible bed will be protected from the turbulence flow. The size of the riprap must be selected so that there are interlocking effects between the rock particles so as to enhance the resistance of removal by fluid motion.

Figure 2-12: Close-up of Riprap

On the other hand, erosion can be inhibited through installation of concrete lining system. This solution will normally be engaged if a devastating scouring is anticipated (i.e. scouring due to plunging jets in plunge pools or overflowing weir). However, failure of liner system will be

inevitable when the designs are not carried out properly. Some of the mechanisms of failure include:

- Thickness of apron is undersized and it does not have the strength to resist the force of the impinging jet.
- Poor design of anchorage where the fluctuation of underlying water pressure causes uplift of protection.
- Insufficient anchorage whereby the scouring depth at the downstream of the apron is greater than the anchorage provided. This allows the removal of erodible sediments which ultimately cause the foundation of the hydraulic structure to fail.

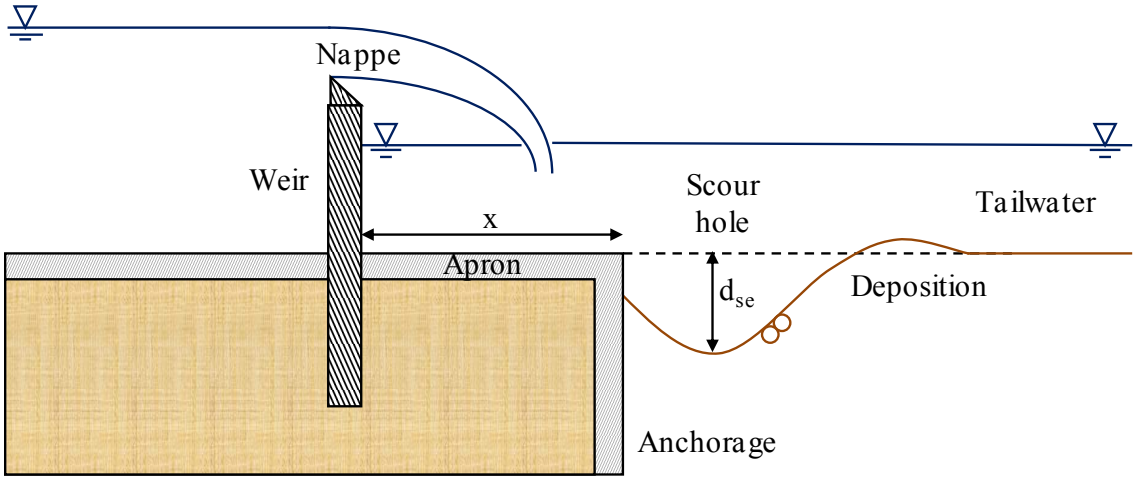

Figure 2-13: Schematic Diagram of Scouring at Downstream of Weir with an Apron

Based on the last failure mechanism, engineers are interested to determine the d_{se} at the end of the apron so that sufficient anchorage can be provided. In addition, (See Figure 2-13) it is also of particular interest to determine the relationship between the apron length, x and d_{se} to provide a cost-effective solution.

2.5 Review of Related Works

Flow over Rectangular Sharp-crested Weir

Bagheri and Heidarpour (2009) used the conventional discharge *Equation (2-1)* for the sharp-crested rectangular weir in their study. Since the concept of critical flow is deemed to be inapplicable for a sharp-crested weir, they have determined the discharge coefficient based on the measured nappe profiles and free-vortex theory. Hence, the function of the discharge coefficient can be represented by the following:

$$C_d = 0.324 \exp\left(0.94 \frac{L_W}{B}\right) \ln\left(1 + \frac{0.73\left(\frac{h}{P}\right) + 3.64}{\exp\left(1.18 \frac{L_W}{B}\right)}\right) \quad (2\text{-}3)$$

In the case of a suppressed weir, $L_W/B = 1$. After comparing the results of the current model with past works, the application of the Equation (2-3) is able to provide acceptable results for $0 < h/P < 9$.

Scour Study

Hoffmans and Verheif (1997) reported that Schoklitsch was one of the earliest who proposed an empirical relationship which is able to define the maximum equilibrium scour depth for a given situation. The equation is given as follows:

$$d_{se} + h_2 = c_s q^{0.57} \Delta h^{0.2} / {d_{90}}^{0.32} \quad (2\text{-}4)$$

Where h_2, tailwater depth; c_s, coefficient with a dimension = 4.75; q, discharge per unit width (m^2/s); Δh, height difference between upstream and tailwater depth (m) and d_{90}, grain size corresponding to 90% finer by dry weight (m). However, Equation (2-4) is recommended for low vertical drop structures where the drop height to water depth upstream of the drop ratio is equal to or less than one.

In the course of his study, some important observations were made:

- Equilibrium scour depth increases with increase in Densimetric Froude Number, Fr_d
- Scour depth decreases with increase in sediment size and tailwater depth.

2.6 Analysis Tools

Sieve Analysis

Sieve analysis is a tool for soil classification. Based on the procedure described by Head (2006), a series of sieves will be first stacked in descending opening order. After which, oven-dried soil sample of known mass is poured into the top sieve and they are then shook with a mechanical shaker. The amount of soil retained on each sieve is weighed. The cumulative percentage finer are then calculated and plotted against the various sieve size.

Soil classification is divided into two main categories, namely coarse-grained and fine-grained. This classification is based on a 0.075mm diameter size sieve as a criterion. If more than half of

the soil sample passed through the 0.075mm sieve, the soil sample is classified as fine-grained and vice versa. Fine-grained is further subdivided into liquid and plasticity limit.

Geometric standard deviation, σ_g is an important parameter to quantify the soil sample gradation.

$$\sigma_g = \sqrt{\frac{d_{84.1}}{d_{15.9}}} \qquad (2\text{-}5)$$

Where,

$d_{15.9} = Grain\ Size\ corresponding\ to\ 15.9\%\ Finer\ by\ Dry\ Weight$

$d_{84.1} = Grain\ Size\ corresponding\ to\ 84.1\%\ Finer\ by\ Dry\ Weight$

Garcia (2007) highlighted that,

$\sigma_g \leq 1.5 \rightarrow$ Sediment bed is uniform

$\sigma_g > 1.5 \rightarrow$ Sediment bed is non-uniform

Dimensional Analysis

Douglas et. al. (2001) highlighted that dimensional analysis is a powerful tool that is frequently used in experimental-based studies where many variables are involved. The main function is to group variables into dimensionless terms that can be easily correlated. The Buckingham Pi Theorem is a key theorem in dimensional analysis. According to the theorem, if an equation involving 'k' number of variables is dimensionally homogeneous, it can be reduced to a relationship with 'k-r' number of dimensionless parameters, where 'r' is the minimum number of basic dimensions required to describe the variables. Dimensionally homogenous signifies that the dimensions on the left and right hand side of the equation are the same.

The dimensionless parameters are called π-terms and they are independent of one another. Using the experimental data obtained, the results of two of these parameters can be fitted on a single curve in which their effects can be clearly presented. The derivation of these parameters does not only provide a means to study the effect on each other individually, regression analysis can be incorporated to correlate a group of dimensionless parameters to a particular interested dimensionless parameter. Section 4.2 will further describe the dimensional analysis conducted for this study.

Modeling and Similitude

The designing of hydraulic structures often requires the use of models. Based on Gerhart and Gross (1985), geometric similar models are often constructed to represent a physical system so that it may be used to predict the behaviors of a desired prototype. The geometry of these physical models is often smaller than its prototype counterpart. For example, a 5m tall prototype can be scaled down by 20:1 so that a 0.25m tall model can be placed conveniently in a laboratory for studies. Nevertheless, the degree of scaling depends on the space and resources available. Due to the geometric similarity, a similar set of dimensionless parameters can be used to study the prototype and its model.

3 Methodology

This Chapter will provide an outline of the experimental set-up and procedures that was carried out to obtain the scour profile for each run.

3.1 Experimental Set-up

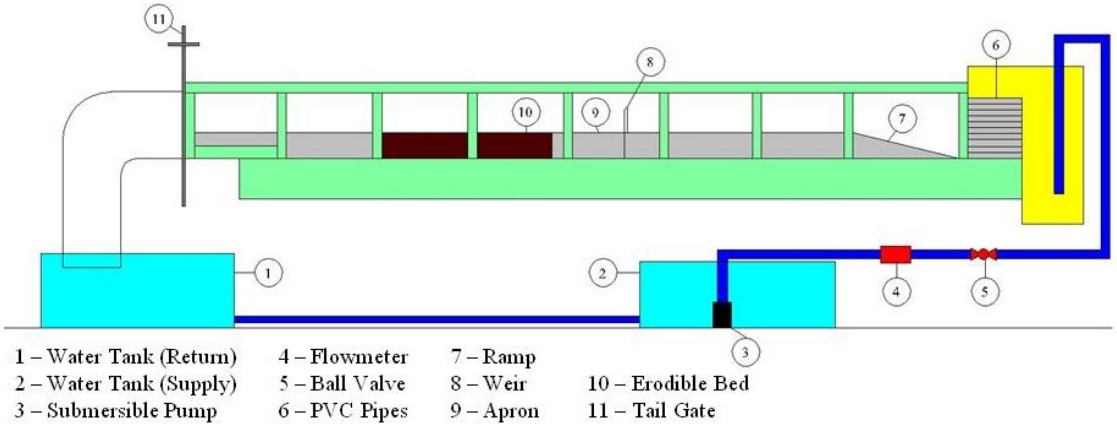

Figure 3-1: Schematic Diagram of Experimental Set-up

The study is being performed by operating an 8.0m long by 0.3m wide by 0.6m deep flume that has an erodible bed of approximately 1.4m long (See Figure 3-1). The flow can be regulated via a ball value and is measured by a flowmeter. The tailwater depth at the downstream of the overflow weir can also be adjusted using a tail gate. The weir height and apron length is alterable as the weir is installed and secured with silicone-gel. In order to obtain the scour profile, clear plastic films were secured along the side of the flume during each run. Permanent markers were used for tracing and followed by manual extraction of data for computerized analysis.

3.1.1 Erodible Bed

The erodible bed is one of the key components in this study. Non-cohesive sand was used in this study and three sets of dry sieve analysis were carried out to determine the uniformity and the median diameter (d_{50}) of the sediment bed. The analysis was conducted for each set whereby 500g of sample was dried at 100°C for 12 hours prior to 30 minutes of sieving. A total of nine sieves (1.40mm, 1.18mm, 1.00mm, 0.85mm, 0.71mm, 0.60mm, 0.50mm, 0.43mm and 0.30mm) and a base pan were arranged in the descending order to determine the size for which the percentage by weight of the material is finer.

The individual results and particle size distribution curves can be obtained from Appendix A. Concisely, $d_{15.9}$, d_{50} and $d_{84.1}$ are tabulated in Table 3-1:

Table 3-1: Summary of Results for Sieve Analysis on Sediment Bed

Percentage Dry Weight Finer by	Size (mm)			
	Set A	Set B	Set C	Average
15.9%	0.86	0.89	0.81	0.85
50.0%	1.10	1.10	1.05	1.08
84.1%	1.30	1.30	1.25	1.28

From the summary of results,

$Median\ Diameter, d_{50} = 1.08mm$

$$Geometric\ Standard\ Deviation, \sigma_g = \sqrt{\frac{d_{84.1}}{d_{15.9}}} = \sqrt{\frac{1.28}{0.85}} = 1.227$$

Since the geometric standard deviation is 1.227 which is smaller than 1.5. The sediment bed is uniform with a d_{50} of 1.08mm.

3.1.2 Computed Weir Discharge

The experiment used a 5mm thick sharp-edged suppressive weir that has a weir height of 100mm. The discharge across the weir can be calculated using Equations (2-1) and (2-3) in which Appendix B shows the detailed calculations.

The following table summarized the comparison between the measured flowrates and the computed weir discharges.

Table 3-2: Comparison between Measured Flowrate and Computed Weir Discharge

Measured Flowrate (L/s)	Computed Weir Discharge (L/s)	Deviation (%)
2.00	1.99	0.50
1.52	1.48	2.63
1.27	1.25	1.57

The comparison between the different sets of flowrate showed that the discharge across the weir only have a deviation of not more than 3% from the measured flowrate. This implies that the discharge measured by the flowmeter and the measured water depth above the weir crest are consistent and reliable to be used in this study.

3.2 Experimental Procedures

Prior Run

1. Set the weir accordingly to the desired weir height and apron length.
2. Started the pump.
3. Topped up water in the water tank to sufficient level whereby the entire submersible pump is below the water table.
4. Adjusted the ball valve so as to regulate the flow to the desired flowrate.
5. Adjusted the tailwater depth to the desired depth.
6. Stopped the pump.
7. Leveled the sediment bed to the same elevation as of the end of the apron.
8. Covered the bed temporary with a metal plate so as to allow the overflow jet to develop prior to commencement of the actual run. This prevented disturbance to the original bed level.
9. Secured clear plastic film along the side of the flume so as to record the scour profiles during the actual run.
10. Recorded the datum of the sediment bed on the clear plastic film.

Actual Run

1. Started the pump.
2. Allowed full development of nappe across the weir.
3. Removed the temporary metal sheet and began to time (t = 0s).
4. Recorded the first profile after t = 30s.
5. Recorded any noticeable changes in profile thereafter for a period of 48 hours (48 hours is the postulated time for the scouring process to reach equilibrium phase, the run can be extended accordingly if necessary).
6. Recorded the scour profile before stopping the pump.
7. Stopped the pump.
8. Recorded the final scour profile.

3.3 Summary of Conducted Experiments

Appendix C gives a tabulation of the Run Log. A total of 28 experiments were conducted in this study whereby the weir height and the type of sediment are fixed throughout the experiment. Apart from the two parameters, the flowrate, tailwater depth and apron length were changed accordingly and the following is a breakdown of the runs and their purpose:

- Four runs (T1~T4) – Trials for the familiarization of the experimental set up and procedures.
- Fifteen runs (W1~W15) – Experiments for the development of scour-time model for free overflowing without bed protection condition.
- Two runs (V1~V2) – Independent runs for the verification of models.
- Seven runs (A1~A7) – Runs for the investigation of effect of varying apron length on equilibrium scour hole; scouring phenomenon was not observed in Run A7.

4 Analysis & Discussion

This Chapter provides a detailed discussion on the general observations of the scour profiles that was made throughout the studies. After which, the emphasis is placed on the modeling of the equilibrium scour time and maximum scour depth as well as the scour-time development relationship. Finally, it provides a brief discussion on the effects of providing an apron on the maximum equilibrium scour depth measured downstream of the apron.

4.1 Observations of Scour Profile

4.1.1 Effects of Varying Flowrate

Figure 4-1 illustrates the scour profiles in the horizontal, L and the vertical, d direction at approximately 48hr of three runs (W3, W9 and W13); the flowrate is the only different parameter among these three runs.

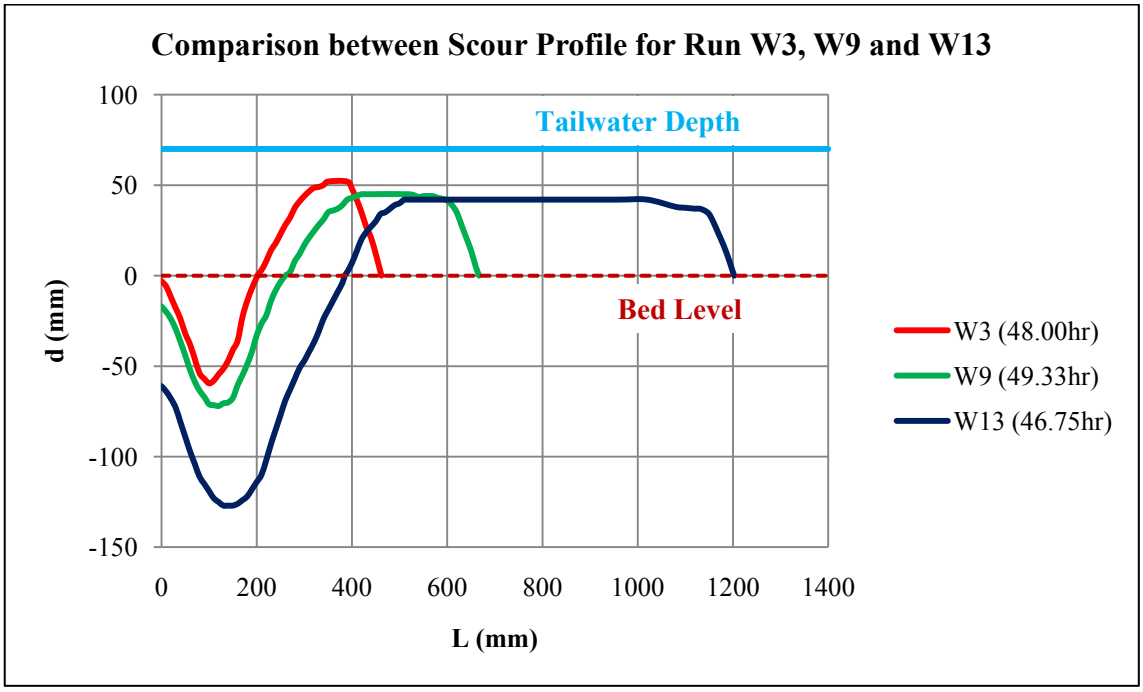

Figure 4-1: Comparison between Scour Profile of Different Flowrate

In general, it can be observed that the scour hole becomes wider and deeper while the ridge deposition deposition became shorter and longer as the flowrate is being increased. From the scour profiles, the the critical scour dimensions can be extracted and they are summarized in Table 4-1: Critical Scour Dimensions of Run at Different Flowrate

. The critical scour dimensions (See Figure 4-2) denote the points that can provide an outline of the shape of the scour hole; they are namely d_b, scour depth at brink; $L`_s$, length at maximum scour depth; $d_s$, maximum scour depth; $L_s$, scour length; $L`_p$, length at maximum deposition

height; d_p, deposition height; L_p, length at the end of deposition and $\frac{d_s}{L_s}$, scour hole geometry ratio.

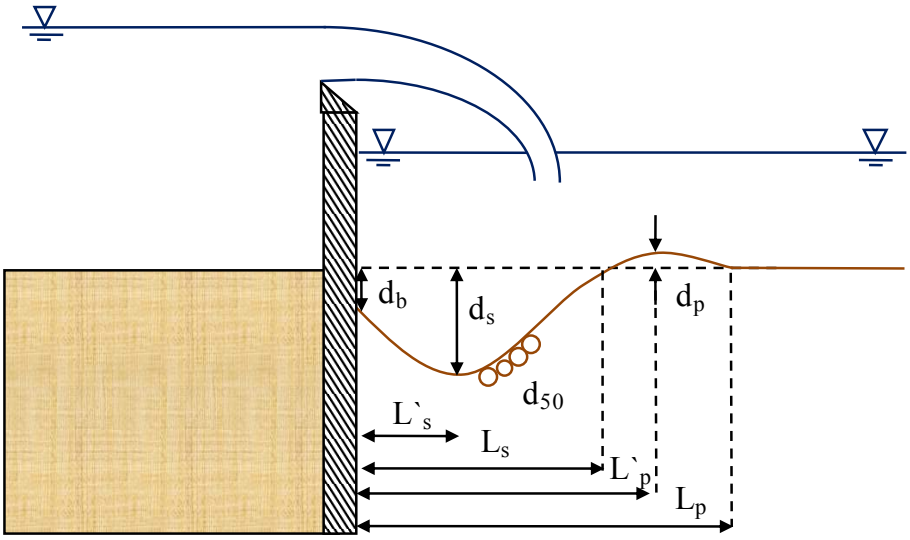

Figure 4-2: Schematic Diagram of Scour Hole with Critical Scour Dimensions

Table 4-1: Critical Scour Dimensions of Run at Different Flowrate

Run	Q (L/s)	t (hr)	d_b	L`$_s$	d_s	L_s	d_s/ L_s	L`$_p$	d_p	L_p
W3	1.27	48.00	-3	100	-60	201	0.30	350	52	462
W9	1.52	49.33	-17	110	-72	260	0.28	420	45	667
W13	2.00	46.75	-61	130	-127	385	0.33	510	42	1203

*Dimensions are in millimeters

By comparing W3 and W9, Table 4-1: Critical Scour Dimensions of Run at Different Flowrate shows that an increase in 20% of Q from 1.27L/s to 1.52L/s will increase the d_s by approximately 20%. On the other hand, comparing W3 and W13, an increase in 57% of Q will increase the d_s by approximately 112%. The above comparison reflects that the increase in flowrate will induce an increase in the maximum scour depth. Based on the open channel flow concept, under constant flow width, the increase in flowrate will lead to larger flow depth and flow velocity. This indicates that the water above the crest of the weir will have a larger potential energy and kinetic energy before it impinges downstream, hence larger eroding capacity. Furthermore, it also implies that the increase in flowrate is not linearly proportional to the increase in the maximum scour depth. Such relationship is also similar for the other critical scour dimensions. This non-linearity might be due to more complex implications.

It can also be observed that the increase in flowrate does not have significant impact on the $\frac{d_s}{L_s}$. The $\frac{d_s}{L_s}$ remained relatively constant even though with the difference in flowrate. This suggests that the change in scour length is proportional to the change in scour depth when flowrate changes.

Table 4-1 also indicates that d_p decreases when Q increases. This implies that the shear stress acting on the deposition is greater since the flow over the deposition increased. Hence, eroding the deposition and reducing the height of the mound. Nevertheless, if the flowrate decrease drastically, the scour will be small and the deposition will be small as well. Thus, this signifies that at certain tailwater depth, there will be a flowrate that will induce the maximum deposition height.

4.1.2 Effects of Varying Tailwater Depth

Figure 4-3 compares the scour profile between W1 and W5 under different tailwater depths. It can be observed that the run with shallower tailwater depth will yield a deeper scour hole.

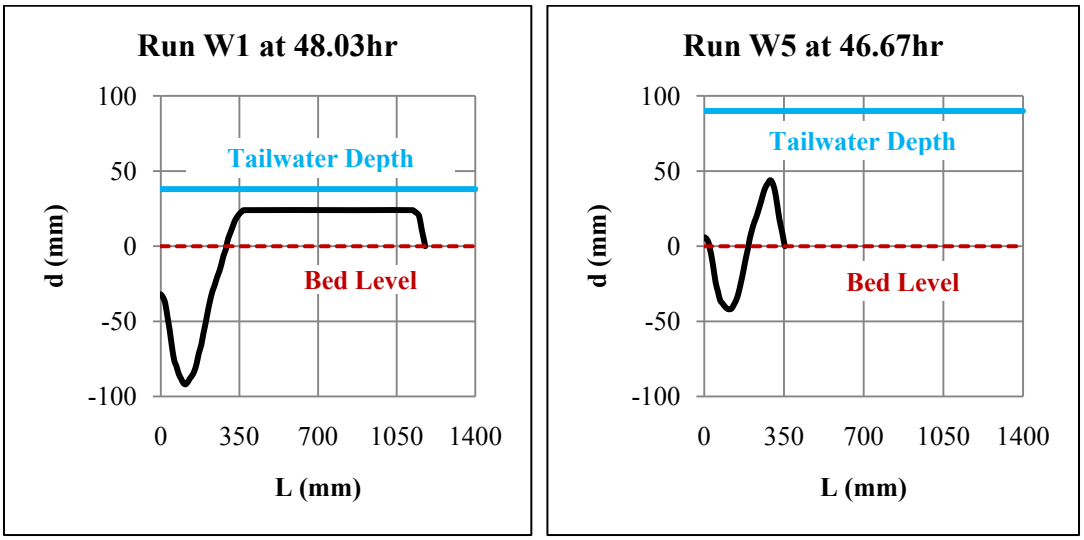

Figure 4-3: Comparison between Scour Profile of Different Tailwater Depth

Table 4-2: Critical Scour Dimensions of Runs at Different Tailwater Depth

Run	Q (L/s)	h_2	t (hr)	d_b	L`$_s$	d_s	L_s	d_s/L_s	L`$_p$	d_p	L_p
W1	1.27	38	48.03	-32	110	-92	292	0.32	370	24	1177
W5	1.27	90	47.67	6	110	-42	194	0.22	290	44	354

*Dimensions are in millimeters

Even though the flowrate of the incoming jet is unchanged, the scour hole still became deeper as the tailwater depth decreases. It is evident from Table 4-2 that an increase in h_2 by 136% caused a 54% d_s reduction. The main reason for this phenomenon is that the barrier to dissipate the energy from the incoming jet is relatively much thicker when tailwater depth increases. This also means that the potential difference between the upstream and downstream water surface is smaller. Therefore, the jet that punches through the deeper tailwater depth hit the erodible bed with a lower velocity and energy, thus creating a smaller degree of erosion.

On the other hand, the increase in h_2 from 38mm in W1 to 90mm in W5 induced a 33% L_s reduction. This changes in L_s was not as drastic as d_s; which caused the $\frac{d_s}{L_s}$ value to decrease from 0.32 to 0.22 when the tailwater depth increases. Therefore, this implies that the changes in the tailwater depth have more significant impacts on the scouring in vertical direction than horizontal direction.

From the measurement of d_p, it can be seen that it increased by 83% when h_2 increased by 136%. This signifies that the tailwater depth is a limiting factor for the height of mound as the surface of the water will act as a boundary that limits its growth.

4.1.3 Effects of Apron Length

Figure 4-4 compares the scour profile at approximately 48hr between the run without apron (W9) and the runs with different apron length (A2 & A5) under the similar flowrate and tailwater depth.

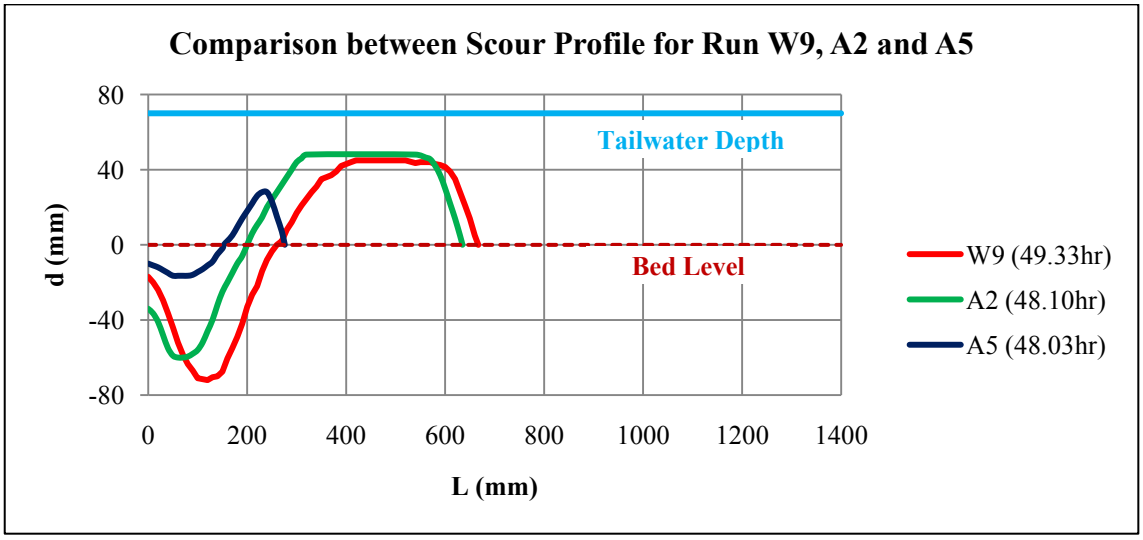

Figure 4-4: Comparison between Scour Profile of Different Apron Length

Table 4-3: Critical Scour Dimensions of Runs with Different Apron Length

Run	Q (L/s)	x	t (hr)	d_b	$L`_s$	d_s	L_s	d_s/ L_s	$L`_p$	d_p	L_p
W9	1.52	0	49.33	-17	110	-72	260	0.28	420	45	667
A2	1.52	100	48.10	-34	60	-60	200	0.30	320	48	635
A5	1.52	350	48.03	-10	50	-17	153	0.11	230	28	276

*Dimensions are in millimeters

From Table 4-3, it can be seen that the scour hole reduced in its size by adding a 100mm long apron at the downstream of the weir. The maximum scour depth and scour length decreased 17% and 23% respectively. Nonetheless, if a 350mm long apron is installed, the maximum scour depth and scour length decreased by 76% and 41% respectively. This signifies that the installation of apron will definitely have impact on the scour formation. In addition, observation of the $\frac{d_s}{L_s}$ shows that the presences of apron has more significant impact on the reduction in d_s than L_s. Furthermore, since the erosion becomes lesser, the deposition formed will be relatively smaller as compared to the experiment without apron.

4.1.4 Effects of Jet Direction

Other than the three different factors in the aforementioned sections that will affect the overall scour profile, there are also two interesting observations made during the experiment and they occurred unintentionally. These two occurrences of scour profile are deemed to be closely related to the jet direction and will be elaborated further.

Jet Flipping

T1 was carried out in a submerged weir condition where the tailwater depth is higher than the weir and Figure 4-5 illustrate the change in the scour profiles at different times.

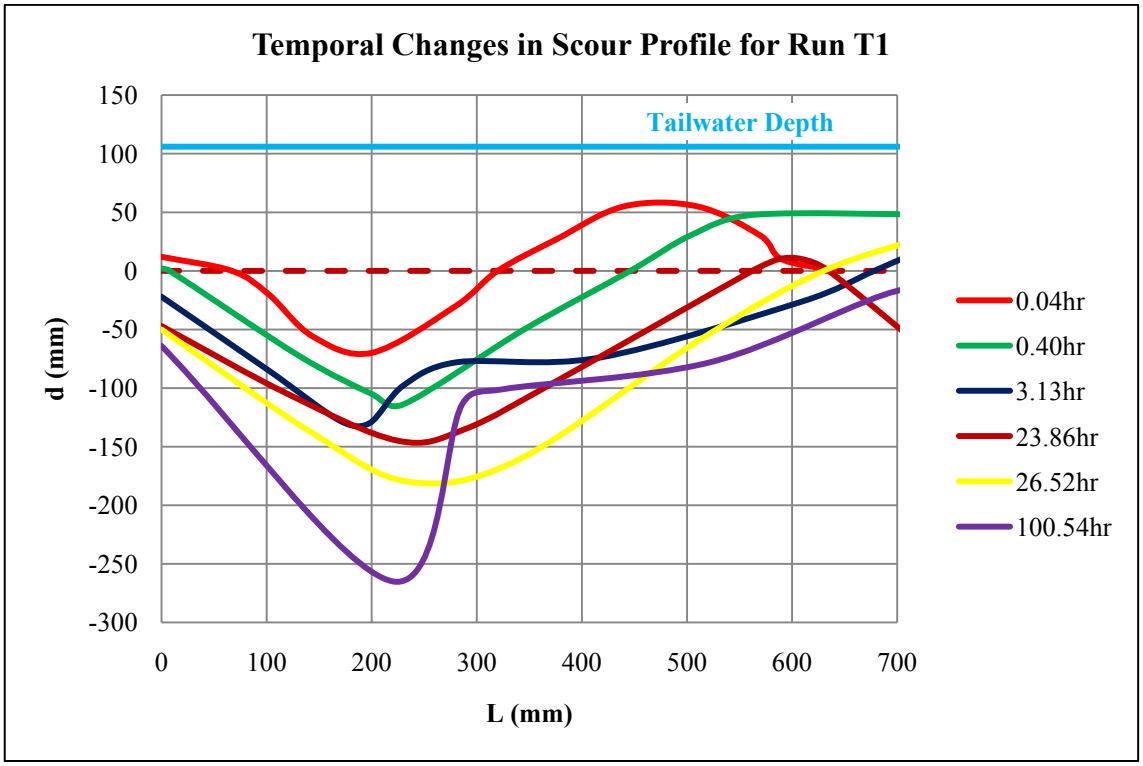

Figure 4-5: Temporal Changes in Scour Profile for Run T1

Through visual inspections, the dimensions of the scour hole from 0.04hr to 0.40hr increased proportionally; such changes signified the scouring process was in the midst of the development stage which fits to the Evolution of Clear-water Scour that is described in *Section 2.3*. However, the scour profile began to transform drastically from 3.13hr onwards in which its shape alternated between "V-shaped scour" (See Figure 4-6) and "Double scour" (See Figure 4-7).

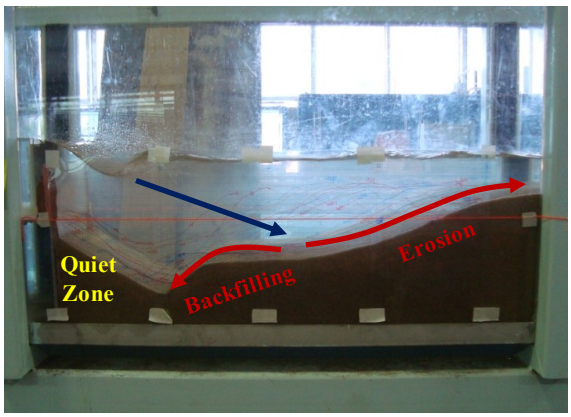

Figure 4-6: V-shaped Scour Profile at 3.13hr

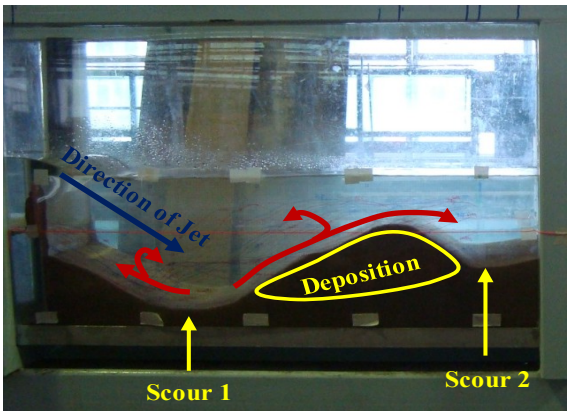

Figure 4-7: Double Scour Profile at 26.52hr

From the real-time observation made during the experiment as shown in Figure 4-6, the overflowing jet from the weir is acting at the downstream of the scour hole; there are no visible vortices observed at the bed of the "Quiet Zone". Nevertheless, the jet that impinged further

downstream caused widening of scour hole and backfilling into a "V-shaped scour". The continuation of such sediment transport eventually led to the evolution of a "Double scour" as shown in Figure 4-7.

During the "Double scour" phase, the jet was observed to tilt steeper towards the bed where the impinging spot shifted nearer to the weir as shown in Figure 4-7. Due to the steeper angle of the jet, the previously backfilled scour was eroded and deposited slightly downstream; this caused the division and two scour holes were formed. These two types of scour hole were observed to recur in a cyclical behavior and were dependent on the overflow jet's direction. This alteration of the jet direction is known as "Jet Flipping".

Clinging Vertical Jet

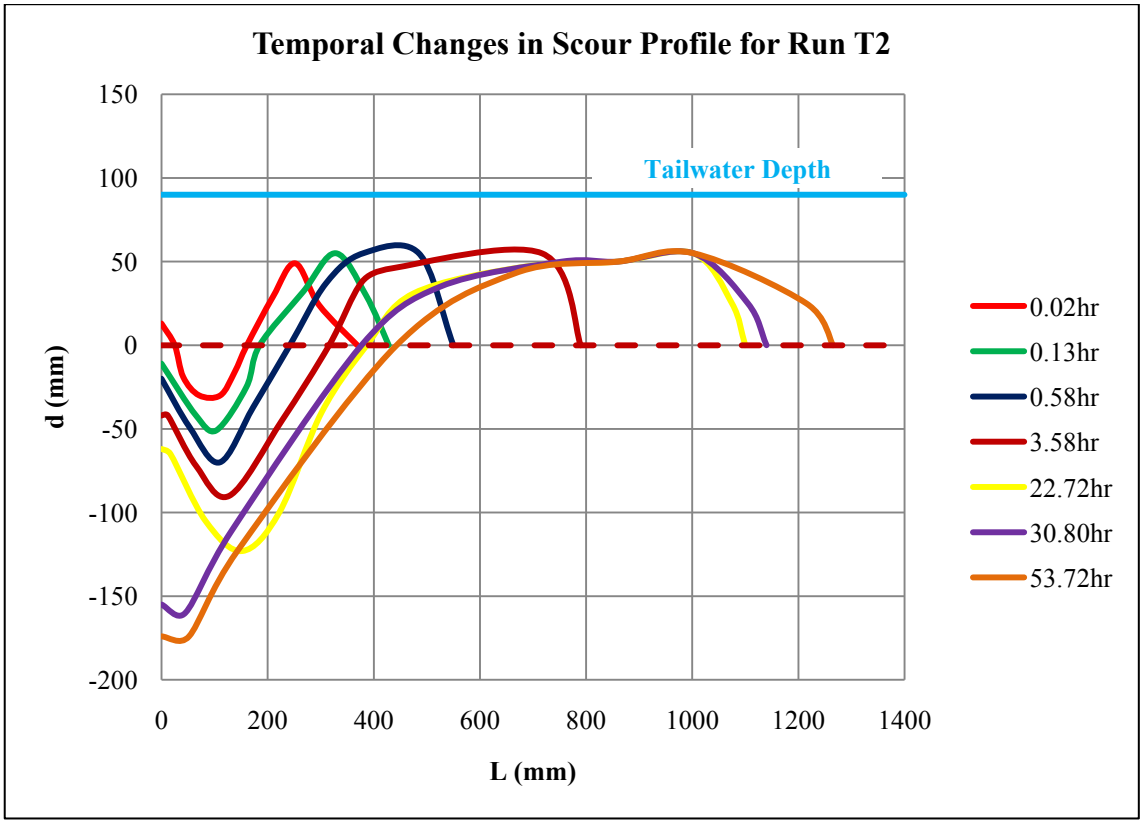

Figure 4-8: Temporal Changes in Scour Profile for Run T2

As shown in Figure 4-8, there was no peculiar occurrence to the scour profiles for 0.02hr to 22.72hr in T2 until the direction of jet changed from an inclined jet to a vertical jet between 22.72hr and 30.80hr; and this caused the scour profile at the upstream to alter tremendously. (See *Figure 4-9* and *Figure 4-10*)

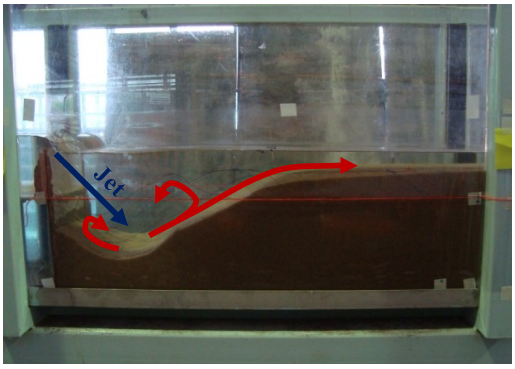

Figure 4-9: Inclined Overflow Jet

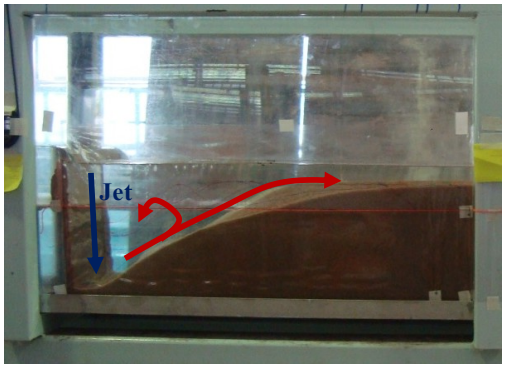

Figure 4-10: Clinging Overflow Jet

When comparing the scour crafted by the two types of jet, the sediments at the downstream of weir (L = 0mm) were transported away as soon as the vertical jet set in; the maximum scour depth shifted upstream. Moreover, based on the relocated maximum scour depth and the observed vortices along the sediment bed, the vertical jet appeared to be clinging to the face of the weir. The clinging of jet is deemed to occur when the flow does not have sufficient energy to spring clear from the crest of the weir. Furthermore, the adherence of jet seemed to be irreversible as the shape of scour profile did not changed from then till the end of the run.

4.2 Dimensional Analysis

With the understanding gained in the experimental observations described above, the next step is to conduct quantitative analysis on the equilibrium scour condition. Aligning to the main objective, the equilibrium scour time and equilibrium maximum scour depth were the two independent variables that are of interest. Figure 4-11 illustrates the scouring phenomenon at the downstream of weir with an apron.

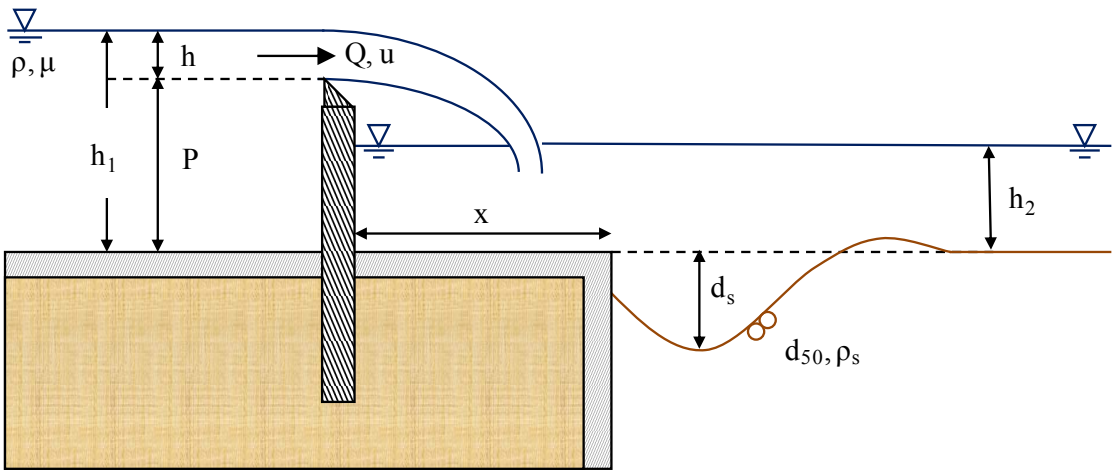

Figure 4-11: Schematic Diagram of Scouring at Downstream of Weir with an Apron

Table 4-4: List of Variables and the Corresponding Dimension

Symbols	Description of Variables	Dimension
t_e	Equilibrium Scour Time	T
d_{se}	Equilibrium Maximum Scour Depth	L
x	Length of Apron	L
P	Height of Weir	L
h_1	Upstream Water Depth	L
h_2	Downstream Water Depth	L
Q	Flowrate	L^3T^{-1}
h	Head of Water above Weir Crest	L
u	Average Flow Velocity above Weir Crest	LT^{-1}
g	Gravitation Acceleration	LT^{-2}
μ	Dynamic Viscosity of Water	$ML^{-1}T^{-1}$
ρ	Density of Water	ML^{-3}
ρ_s	Density of Sediment	ML^{-3}
d_{50}	Median Particle Diameter	L

A total of twelve dependent variables of different aspects were identified and deemed to have influence on the equilibrium condition in which:

$$(t_e \ or \ d_{se}) = f_1(x, P, h_1, h_2, Q, h, u, g, \mu, \rho, \rho_s, d_{50}) \tag{4-1}$$

Using dimensional analysis, see Appendix D for the derivation, the followings are the dimensionless π-terms:

$$\left(\frac{t_e g^{0.5}}{h^{0.5}} \ or \ \frac{d_{se}}{h}\right) = f_2\left(\frac{x}{h}, \frac{h_1}{h}, \frac{h_2}{h}, \frac{Q}{g^{0.5}h^{2.5}}, \frac{P}{h}, Fr = \frac{u}{\sqrt{gh}}, \frac{h^{1.5}g^{0.5}\rho}{\mu}, S = \frac{\rho_s}{\rho}, \frac{d_{50}}{h}\right) \tag{4-2}$$

Two common dimensionless parameter were obtain from the derivation; they are namely Froude Number, Fr and Specific Gravity of Sediment, S. By conducting preliminary assessment, some of the dimensionless dependent terms can be fused together in order to present a more significant meaning to the study. The following will describe three fusions of dimensionless terms:

Water Depth Ratio

In view of physical reasoning, the resultant scour geometry for a given tailwater depth will increase with upstream water depth; larger upstream water depth possesses greater potential

energy for scouring. Conversely, by fixing the upstream water depth, the resultant scour hole will decrease in size with increasing tailwater depth. Since jet will lose its momentum along its travelled path, the tailwater essentially functions as a buffer for the impinging jet to dissipate its energy before it strikes the erodible bed.

As the development of scour hole is significantly dependent on these two water depths, the fusion of these two variables will be able to show a better correlation between the water depths and the depth of the scour hole. Hence, the π-terms can be combined by taking the difference in which the non-dimensional parameter will become $\Delta h/h$; $\Delta h = h_1 - h_2$. This π-term signifies that the difference in the water elevation will be responsible for the magnitude of scour development; the scour will be larger when the difference is greater and this is true according to the observations made earlier.

Nonetheless, the aforementioned will only apply in the event when free overfall from the weir is present. When h_1 becomes very large, the weir will be flooded and h_2 will approach h_1. This is also similar if h_2 is very large. At these instances, the effect of jet scouring will no longer be dominant since $\Delta h \to 0$.

Densimetric Froude Number

Fr is a dimensionless number that compares the inertia force with the gravitational force. However, as indicated by Dey and Raikar (2007), it is more appropriate to represent the sediment-water interaction with the Densimetric Froude Number, Fr_d . Fr_d is more representative in this study as the effect of buoyancy has to be accounted in the midst of the sediment transport during scouring. Hence, apart from including the ratio of density difference, d_{50} will be more suitable than h as the 'length' scale since the particle size is deemed to has a greater influence on the Fr_d.

The following shows the derivation of Fr_d:

$$\frac{u}{\sqrt{gh}} \times \frac{1}{\sqrt{S-1}} \times \frac{1}{\sqrt{\frac{d_{50}}{h}}} = \frac{u}{\sqrt{g(S-1)d_{50}}} = Fr_d \tag{4-3}$$

Reynolds Number

Reynolds Number, Re is a dimensionless number that is commonly used to quantify the ratio of inertia force to viscous effect within a fluid flow. $\frac{h^{1.5} g^{0.5} \rho}{\mu}$ from the earlier derivation contain the

ratio of density to viscosity; similar to Re. Hence, replacing g with u is more representative of the inertia force with the flow. This can be achieved by the following fusion:

$$\frac{h^{1.5}g^{0.5}\rho}{\mu} \times \frac{u}{\sqrt{gh}} = \frac{hu\rho}{\mu} = Re \tag{4-4}$$

From the fusion, Equation (4-2) can be re-written into:

$$\left(\frac{t_e g^{0.5}}{h^{0.5}} \; or \; \frac{d_{se}}{h}\right) = f_3\left(\frac{x}{h}, \frac{\Delta h}{h}, \frac{Q}{g^{0.5}h^{2.5}}, \frac{P}{h}, Fr_d, Re\right) \tag{4-5}$$

4.3 Scour-Time Development Relationship

The scour-time development relationship denotes the temporal changes in the maximum scour depth; it is an important component in this study. This relationship can be obtained by plotting the maximum scour depth, d_s with its corresponding time, t that is obtained from each run. This relationship can help to predict and extrapolate the development of maximum scour depth for each run. Figure 4-12 shows an example of the scour-time development curve that is plotted using the data collected from Run W1.

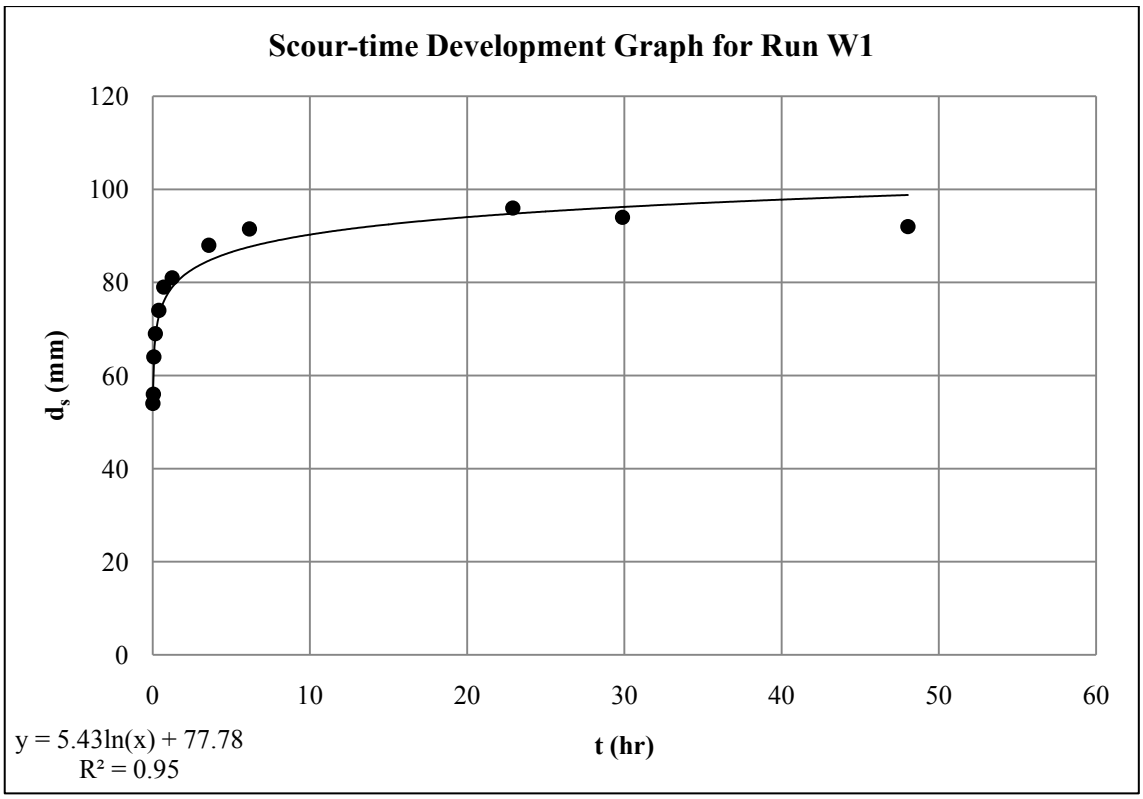

Figure 4-12: Example of Scour-time Development Graph for Run W1

Appendix E consolidates the scour-time development graphs for the fifteen runs without apron and six runs with apron. In general, the graphs show that the maximum scour depth increases indefinitely with time. The rate of increment is tremendous at the beginning of the run while the rate slowed down as the experiment proceeded on. From the development, the scour-time relationship for the individual graph can be obtained by fitting a log-type trendline to the data points. Since the R^2 value for the graphs are greater than 0.9 except for Runs A3, A4 and W7, the trendline are believed to be useful for extrapolation to the long time value of d_s. Hence, it is reliable to use these relationships for further analysis.

4.4 Determination of Equilibrium Scour Time and Equilibrium Maximum Scour Depth

In order to correlate the π-terms in Equation (4-5), the values t_e and d_{se} must be known for each run. The purpose of this section is to elaborate the method to determine the values of t_e and its corresponding d_{se} in this study. Highlighted in the previous section, the time of equilibrium signifies the point whereby the scour hole does not have visible changes; nevertheless it is impossible to determine this exact instant through visual observation during the experiment. The main reason is that physical observation is a subjective process in which the same person will estimate things differently at different instance; and even more subjective for different individual. Therefore, if the time of equilibrium is determined through observation only, the results will be inconsistent for future comparison.

Aborting the "visual" approach, this study would like to propose the "Predetermined Equilibrium Scour Rate" approach. Equilibrium scour rate is defined as the speed of erosion relative to the maximum scour depth. Theoretically, it is known that equilibrium phase will only begin when $\frac{d(d_s(t))}{dt} = 0$, and this will occur if the experimental time stretches for a considerably long period (i.e. conducting each run for few hundred hours). However, it is impossible to achieve this practically due to the limitation of time in this study. Therefore, a reasonable $\frac{d(d_s(t))}{dt}$ can be assumed to represent the equilibrium condition. Hence, $\frac{d(d_s(t))}{dt} = 0.2mm/hr$ is chosen in this study. Physically, $\frac{d(d_s(t))}{dt} = 0.2mm/hr$ is equivalent to a change of 1mm in depth within a period of 5hr; whereby 1mm is the smallest measurable length scale in the experiment and 5hr is the approximate time interval of data recording.

In order to obtain the values of t_e and d_{se} for each run, the scour-time curve in Section 4.3 can be used. As an example, the log-type curve for W1 is,

$$d_s(t) = 5.43\ln(t) + 77.78 \quad (4\text{-}6)$$

By differentiating the above relationship, the scour rate function for W1 is,

$$\frac{d(d_s(t))}{dt} = \frac{5.43}{t} \quad (4\text{-}7)$$

Next, the rate function can be equated to the "Predetermined Equilibrium Scour Rate" for the determination of t_e,

$$\frac{5.43}{t_e} = 0.2mm/hr \rightarrow t_e = 27.1hrs \quad (4\text{-}8)$$

Lastly, the corresponding d_{se} can be calculated by substituting t_e into the scour-time relationship as shown in Equation (4-6),

$$d_{se} = 5.43\ln(27.1) + 77.78 = 95.7mm \quad (4\text{-}9)$$

Appendix F tabulates the rate function, t_e and d_{se} for the 15 experiments without apron and six experiments with apron. The tabulated results shows that each run has its unique rate function, t_e and d_{se}. This is mainly due to the difference in the operating conditions for the individual run. Nevertheless, they do exhibit trend that are in conjunction with the change in flowrate and tailwater depth. In short, increasing in flowrate and decreasing in tailwater depth will result in a larger scouring rate, longer t_e and deeper d_{se}.

Nevertheless, Appendix F also compares the percentage deviation between the calculated d_{se} with the actual maximum scour depth corresponding to the end of the experiment, d_{sf} for each of the individual run. The results show that the average deviation is 3.42% for no-apron condition is and 11.78% for apron condition. This indicates that the "Predetermined Equilibrium Scour Rate" method is reliable.

4.5 Similarity of Scour-time Curves

Using the values of t_e and the corresponding d_{se} that was determined from the "Predetermined Equilibrium Scour Rate" method in the previous section, the scour-time development curves can be normalized by plotting $\frac{d_s}{d_{se}}$ against $\frac{t}{t_e}$. Figure 4-13 shows the normalized graphs for three runs that is conducted with different flowrate and tailwater depth. From the plot, it can be seen that the effects of the two parameters on scour-time curves are similar.

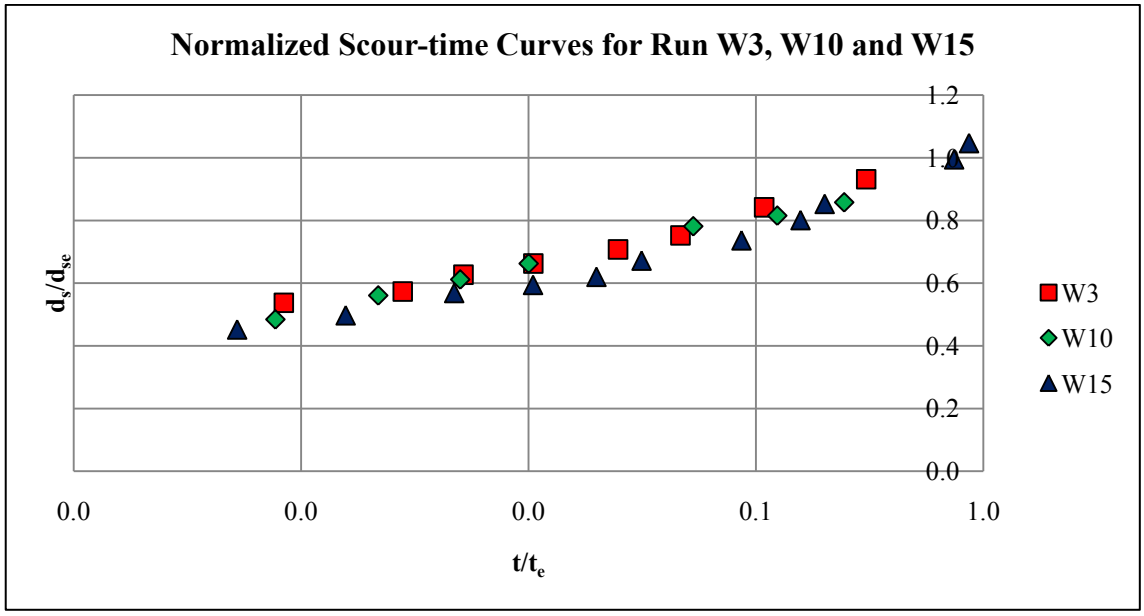

Figure 4-13: Similarity of Normalized Scour-time Curves

In addition, it can be observed that the scour depth increases very rapidly in the early stage. The normalized curves illustrate that 60% of d_{se} could be reached within 2% of t_e when the run commenced. Furthermore, at 20% of t_e, almost 90% of the d_{se} can be attained.

Figure 4-14 shows the normalized $\frac{d_s}{d_{se}}$ and $\frac{t}{t_e}$ for the 15 runs without apron (W1~W15) plotted on a log-log scale.

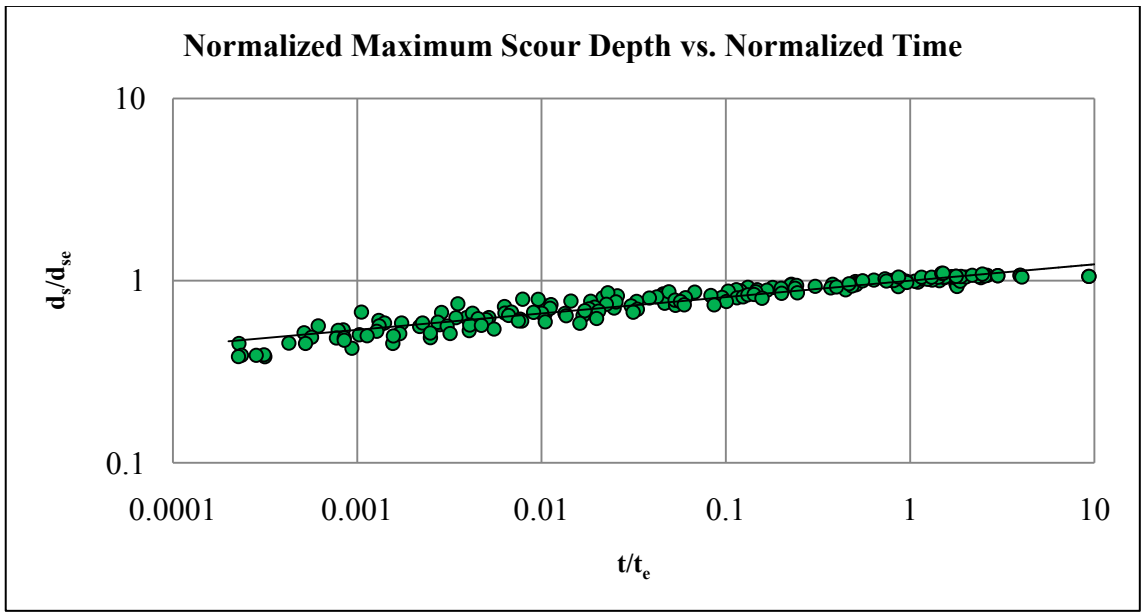

Figure 4-14: Normalized Maximum Scour Depth against Time Graph

From the plot, the correlation between the two normalized ratios is established whereby:

$$\frac{d_s}{d_{se}} = \left(\frac{t}{t_e}\right)^{0.09} \tag{4-10}$$

The above function will be used in Section 4.7 for the modeling of scour-time development.

4.6 Prediction of Equilibrium Scour Time and Equilibrium Maximum Scour Depth

With t_e and d_{se} that are determined in Section 4.4, they can be fitted into Equation (4-5) for regression analysis. However, before getting on with the analysis, some of the terms can be ignored. Three terms can be ignored in this analysis includes:

- x/h – Without apron condition ($x = 0$)
- P/h – Weir height is unchanged throughout the study
- Re – Study only involved in the turbulent flow regime

Hence, Equation (4-5) is reduced to the following:

$$\left(\frac{t_e g^{0.5}}{h^{0.5}} or \frac{d_{se}}{h}\right) = f_4\left(\frac{\Delta h}{h}, \frac{Q}{g^{0.5}h^{2.5}}, Fr_d\right) \tag{4-11}$$

Through regression analysis (See Appendix G – Part 1), Equations (4-12) and (4-13) are determined:

$$\frac{t_e g^{0.5}}{h^{0.5}} = 4.52\left(\frac{Q}{g^{0.5}h^{2.5}}\right)^{2.16} {Fr_d}^{10.74}\left(\frac{\Delta h}{h}\right)^{0.75} \tag{4-12}$$

$$\frac{d_{se}}{h} = 0.89\left(\frac{Q}{g^{0.5}h^{2.5}}\right)^{-0.49} {Fr_d}^{2.61}\left(\frac{\Delta h}{h}\right)^{0.86} \tag{4-13}$$

The values of $\frac{t_e g^{0.5}}{h^{0.5}}$ and $\frac{d_{se}}{h}$ were computed and the error incurred is within ±15% when they are plotted against the measured data; the average error is smaller than ±1%. This implies that the equations can provide a good predictability of the equilibrium scour time and maximum scour depth. However, $\frac{Q}{g^{0.5}h^{2.5}}$ seems to have a replicated effect in terms of the flow since Fr_d already encompassed the flow effect. Therefore, $\frac{Q}{g^{0.5}h^{2.5}}$ can be removed and another regression analysis

can be conducted to determine a new set of equilibrium equations. Hence, without $\frac{Q}{g^{0.5}h^{2.5}}$ (See Appendix G – Part 2), Equations (4-14) and (4-15) are the new sets of equilibrium equations:

$$\frac{t_e g^{0.5}}{h^{0.5}} = 11281 Fr_d{}^{6.47} \left(\frac{\Delta h}{h}\right)^{0.78} \quad for\ 1.8 \le Fr_d \le 2.2; 1.4 \le \frac{\Delta h}{h} \le 4.7 \tag{4-14}$$

$$\frac{d_{se}}{h} = 0.15 Fr_d{}^{3.59} \left(\frac{\Delta h}{h}\right)^{0.85} \quad for\ 1.8 \le Fr_d \le 2.2; 1.4 \le \frac{\Delta h}{h} \le 4.7 \tag{4-15}$$

With the above equations, the values of $\frac{t_e g^{0.5}}{h^{0.5}}$ and $\frac{d_{se}}{h}$ were computed again and the error incurred is also within ±15% when they are compared against the measured data (See Figure 4-15 and Figure 4-16). This proved that the earlier assumption whereby $\frac{Q}{g^{0.5}h^{2.5}}$ is redundant is positive in the analysis.

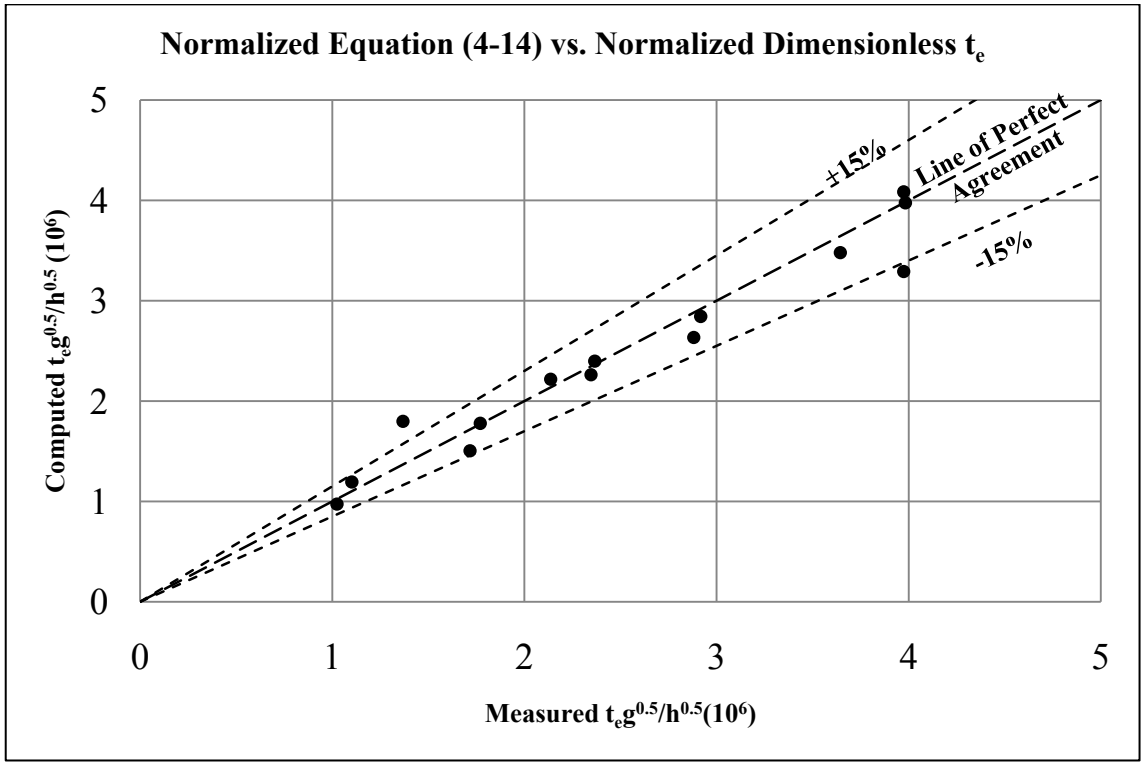

Figure 4-15: Comparison between Computed and Measured Dimensionless Equilibrium Scour Time

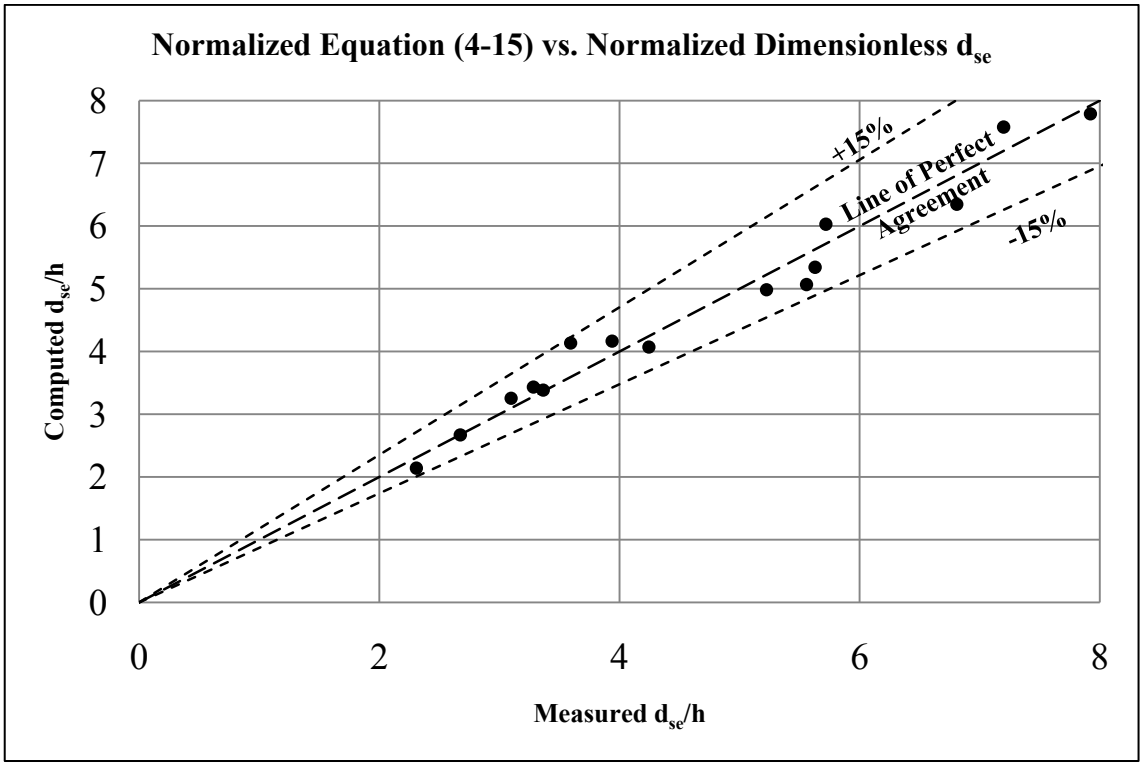

Figure 4-16: Comparison between Computed and Measured Dimensionless Equilibrium Maximum Scour Depth

Re-writing Equations (4-14) and (4-15),

$$t_e = 3602h^{0.5}Fr_d{}^{6.47}\left(\frac{\Delta h}{h}\right)^{0.78} \quad for\ 1.8 \le Fr_d \le 2.2; 1.4 \le \frac{\Delta h}{h} \le 4.7 \tag{4-16}$$

$$d_{se} = 0.15hFr_d{}^{3.6}\left(\frac{\Delta h}{h}\right)^{0.85} \quad for\ 1.8 \le Fr_d \le 2.2; 1.4 \le \frac{\Delta h}{h} \le 4.7 \tag{4-17}$$

Equations (4-16) and *(4-17)* show that Fr_d plays a prevailing role in the prediction of t_e and d_{se}.

Nevertheless, to reinforce the predictability of Equations (4-16) and (4-17), two independent verifications runs (V1 and V2) were conducted. The values of t_e and d_{se} were calculated using *Equations (4-16) and (4-17) and the* results are tabulated in Table 4-5.

Table 4-5: Comparison between Actual Maximum Scour Depth and Calculated Equilibrium Maximum Depth

Run	(1)	(2)	(3)	(4)
	Calculated t_e (hr) *Equation (4-16)*	**Calculated d_{se} (mm) *Equation (4-17)***	**Extrapolated d_{se} at 50t_e (mm)**	**(2)/(3) (%)**
V1	38.46	103.4	121.5	85
V2	20.82	69.5	87.7	79

The calculated d_{se} in Column (2) of Table 4-5 was then used to compare with the d_{se} in Column (3) that was calculated using the actual scour-time relationship at 50 times of the calculated t_e. The comparison shows that the calculated d_{se} is able to return almost 80% of the extrapolated d_{se}. This implies that *Equations (4-16)* and *(4-17)* are reliable and able to provide quite a good representative prediction if they are used.

4.7 Prediction of Scour-time Development

By substituting the *Equations (4-16)* and *(4-17)* into *Equation (4-10)*, the scour-time model can be achieved for $1.8 \leq Fr_d \leq 2.2$ and $1.4 \leq \frac{\Delta h}{h} \leq 4.7$:

$$d_s = 0.06h^{0.955} g^{0.045} {Fr_d}^3 \left(\frac{\Delta h}{h}\right)^{0.78} t^{0.09} \quad (4\text{-}18)$$

Figure 4-17 shows the comparison between dimensionless Equation (4-18) with the actual dimensionless measured data in semi-log scale and they demonstrated good prediction. The dimensionless Equation (4-18) is obtained by dividing the maximum scour depth calculated from Equation (4-18) with the equilibrium maximum scour depth calculated by Equation (4-17). Appendix H tabulates the comparison for all the runs with no apron.

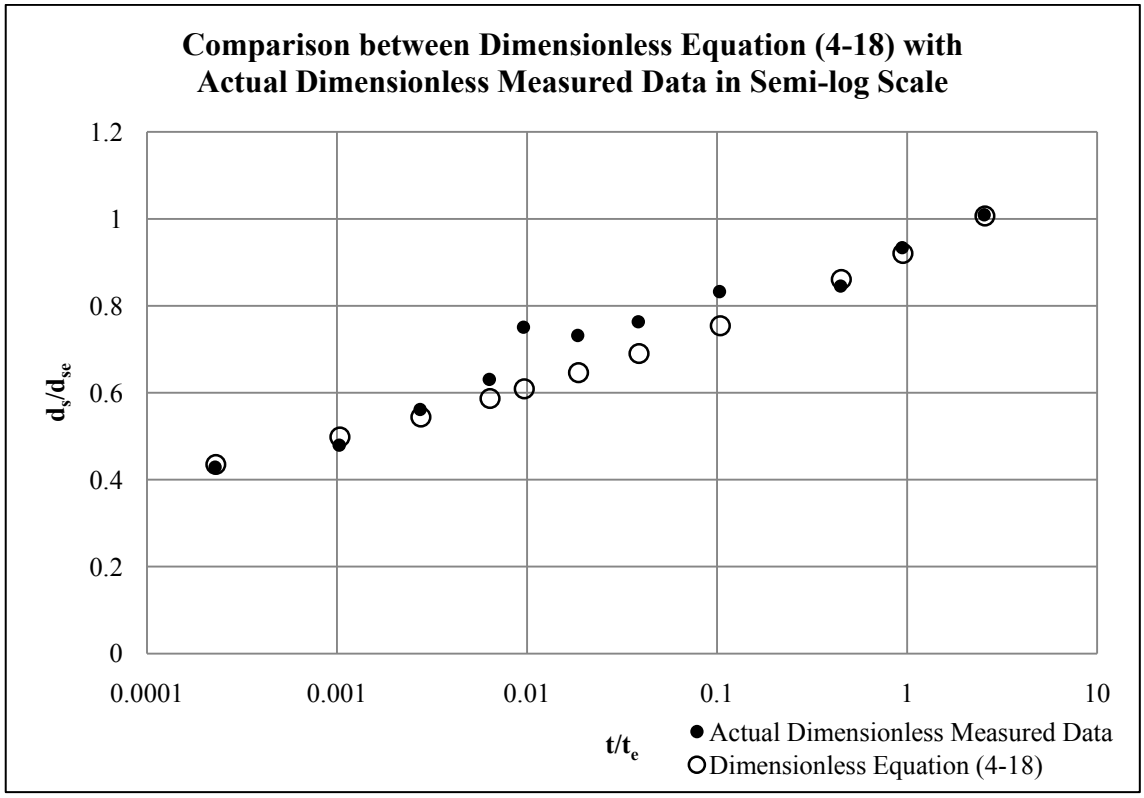

Figure 4-17: Comparison between Dimensionless Equation (4-18) with Actual Dimensionless Measured Data in Semi-log Graph

Furthermore, the predictability of Equation (4-18) can be reinforced by using the data collected from the verifications runs. Figure 4-18 displays that Equation (4-18) is able to provide a substantial prediction of the scour-time development.

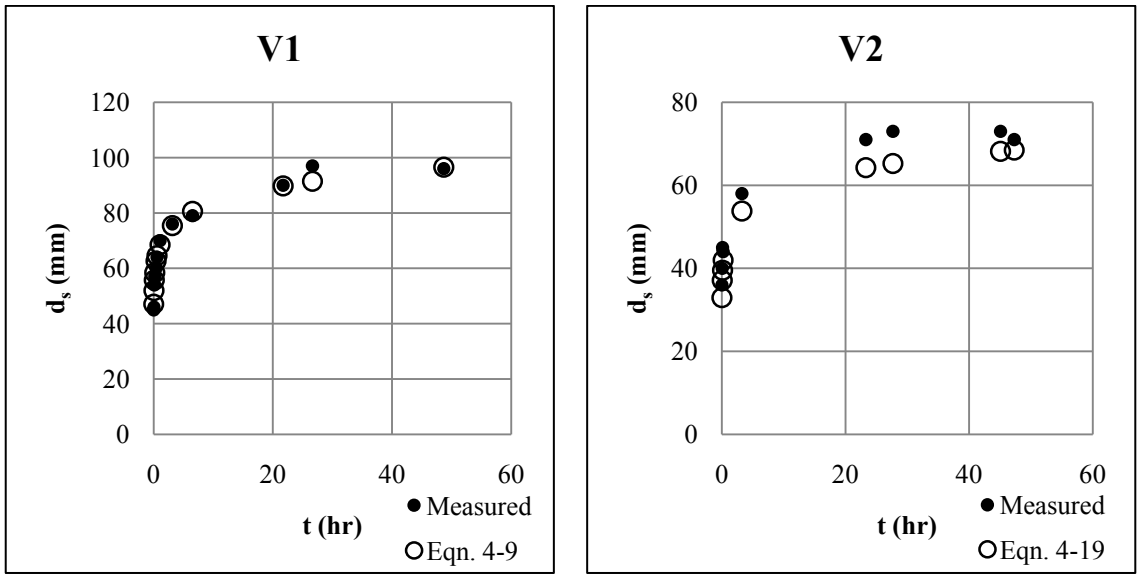

Figure 4-18: Comparison of Measured Data with Eqn. 4-19 for Verification Runs

By examining *Equation (4-18)*, it can be observed that the effect of Fr_d is more dominant than $\frac{\Delta h}{h}$ in the scour formation. Nevertheless, both of the terms fitted the description that is highlighted in Section 4.1 such that an increase in flowrate or increase in the water depth difference will result in a larger maximum scour depth. However, a point to note is that the sediment properties of the erodible bed is unchanged for the present experiments. More study should be done with different d_{50} in Fr_d.

4.8 Correlation of Apron Length and Equilibrium Maximum Scour Depth

As mentioned in the earlier section, apron of various length are installed to understand its effect on the development of equilibrium maximum scour depth. Since only x is varied in this section of investigation, Equation (4-5) can be reduced to the following:

$$\left(\frac{t_e g^{0.5}}{h^{0.5}} or \frac{d_{se}}{h}\right) = f_5\left(\frac{x}{h}\right) \tag{4-19}$$

In order to magnify and understand the effect of apron on the equilibrium condition, the 'Predetermined' values of $\frac{t_e g^{0.5}}{h^{0.5}}$ and $\frac{d_{se}}{h}$ for A1 to A7 with apron can be normalized with the "Predetermined' values of $\frac{t_e g^{0.5}}{h^{0.5}}$ and $\frac{d_{se}}{h}$ for no-apron Run W9 respectively, and then plotted against $\frac{x}{h}$ as shown in Figure 4-19 and Figure 4-20. Run W9 is used for the normalization as it has the similar operating conditions as Run A1 to A7. It can be seen that the equilibrium condition of A1 ($\frac{x}{h} = 2.63$ whereby $x = 50mm$) did not exhibit any influence by the presence of apron. The reason may be due to the fact that the nappe sprang further than the apron length, thus it still impinges directly onto the erodible bed creating scour that is comparable to the no apron case of W9. Next, it can be observed that as soon as $\frac{x}{h}$ approaches 15 (where x is between 300mm to 500mm), the equilibrium condition decreased to approximately 20% of the no apron case of W9. As $\frac{x}{h}$ approaches 26, no visible scouring is observed. Using the 'Predetermined' From the above, a simple correlation can be established using the data from A2 to A6 in which:

$$\frac{t_e g^{0.5}}{h^{0.5}} = 10^{7.1}\left(\frac{x}{h}\right)^{-1.24} for\ 5.5 \leq \frac{x}{h} \leq 18 \tag{4-20}$$

$$\frac{d_{se}}{h} = 35.22\left(\frac{x}{h}\right)^{-1.51} for\ 5.5 \leq \frac{x}{h} \leq 18 \tag{4-21}$$

Equations (4-20) and (4-21) can be normalized with the values of Run W9 and is plotted on Figure 4-19 and Figure 4-20.

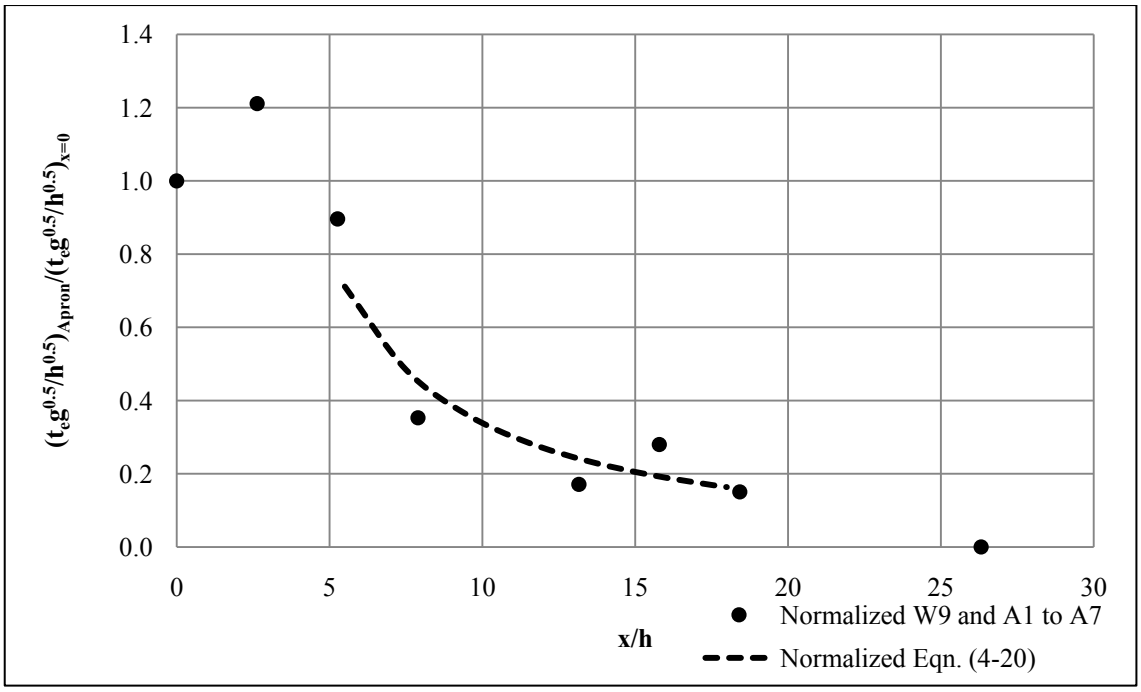

Figure 4-19: Normalized Equilibrium Scour Time against Dimensionless Apron Length

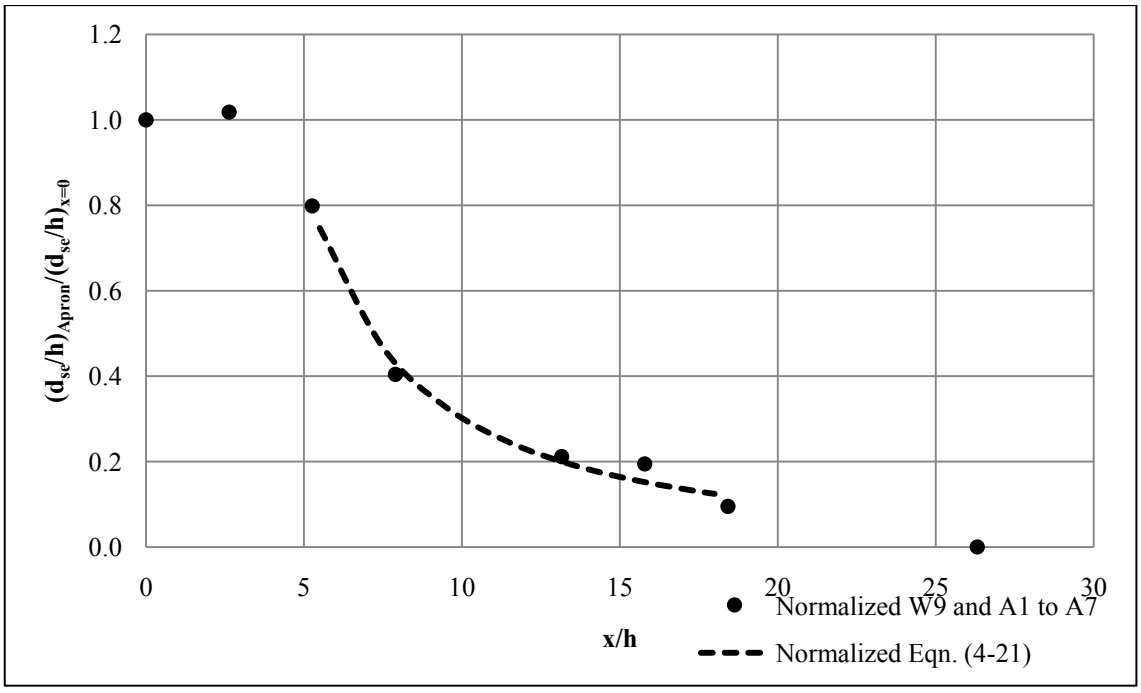

Figure 4-20: Normalized Maximum Equilibrium Scour Depth against Dimensionless Apron Length

5 Conclusion

This study shows that the scouring dynamics at the downstream of the overflowing weir with and without an apron are greatly affected by the flowrate, water depths, apron length and the overflowing jet direction into the water body. The observations made on the scour profiles showed that the maximum equilibrium scour depth will increase when flowrate increases, tailwater depth decrease and apron length decreases.

After understanding some of the key parameters that will affect scouring, attention were being placed on the prediction of equilibrium scour time and maximum scour depth. A "Predetermined Equilibrium Scour Rate" method is proposed in this study to determine the equilibrium condition of the conducted experiments. The results show that the average deviation between the "Predetermined" depth and the actual final scour depth is 3.42% for no-apron condition and 11.78% for apron condition. Hence, the "Predetermined Equilibrium Scour Rate" method is reliable.

The equilibrium scour time and the equilibrium maximum scour depth were correlated with Densimetric Froude Number and Water Depth Ratio and a set of predictive equations are proposed. The verifications runs proved that these Equations were feasible to estimate the equilibrium maximum scour depth since the prediction is approximately 80% of the actual extrapolated maximum scour depth. The equilibrium relationships were further combined with the normalized scour-time relationship to track the temporal change in the scour development. Once again, the verifications proved that the predictability of the equations is within a satisfaction limit.

The investigation of the influence of apron length reflected that a minimum apron length must be presence in order to effectively intercept the nappe from the erodible bed. In addition, when the ratio of apron length to the height of water depth above the crest approaches 15, the equilibrium maximum scour depth can be reduced by 80%.

6 Recommendations

In this study, the Densimetric Froude Number can only captured the effect of the varying flowrate. Future studies can be carried out by employing a wider range of sediment to strengthen this dimensionless term.

Next, the flowrate chosen is bounded by the depth of the sediment bed. Larger flowrate will implies deeper scour depth; hence, if a larger flowrate is chosen, the erosion capacity will be so large that it will scour to the bottom of the flume. This will cause a limitation in the data recording. This also applies if the weir height is too high. Hence, in order to study a larger scale of flowrate or weir height, the tailwater depth or sediment size must be scaled up accordingly. Otherwise, the flume can be modified with deeper sediment depth.

The bottom of the nappe is not ventilated in this study. This might cause some degree of fluctuation in the jet direction when water depth beneath the nappe changes since it has to maintain the pressure in an enclosed volume; consequently affecting the scour profile. Hence, ventilation should be provided in the future.

References

Akan, A. O. (2006). Open Channel Hydraulics. Canada: Elsevier.

Annandale, G. W. (2006). *Scour Technology Mechanics and Engineering Practice.* New York: McGraw-Hill.

Azimi, A. H., & Rajaratnam, N. (2009). Discharge Characteristics of Weirs of Finite Crest Length. *Hydraulic Engineering* , 1081-1085.

Bagheri, S., & Heidarpour, M. (2009). Flow Over Rectangular Sharp-crested Weirs. *Irrigation Science* , 173-179.

Chien, N., & Wan, Z. (1999). *Mechanics of Sediment Transport.* USA: ASCE.

Dey, S., & Raikar, R. V. (2007). Scour below a High Verticle Drop. *Journal of Hydraulic Engineering* , 564-568.

Douglas, J. F., Gasiorek, J. M., & Swaffield, J. A. (2001). *Fluid Mechanics.* Essex: Prentice Hall.

Garcia, M. H. (2007). *Sedimentation Engineering: Process, Measurements, Modeling, and Practice.* Virginia: ASCE.

Gerhart, P. M., & Gross, R. K. (1985). *Fundamentals of Fluid Mechanics.* Canada: Addison-Wesley.

Graf, W. H. (1998). *Fluvial Hydraulics.* United Kingdom: Wiley.

Head, K. H. (2006). *Manual of Soil Laboratory Testing Volume 1: Soil Classification and Compaction Tests.* Caithness: CRC Press.

Hoffmans, G., & Verheif, H. (1997). Scour Manual. Netherlands: A.A. Balkema.

Jain, S. C. (2001). Open Channel Flow. USA: John Wiley & Sons, Inc.

Appendix A Results of Sieve Analysis

Set A

S/N	Sieve Size (micron)	Empty Sieve Weight (g)	Filled Sieve Weight (g)	Sand Weight (g)	% Retain	% Coarser	% Finer
1	1.40	408.5	412.6	4.1	0.8	0.8	99.2
2	1.18	400.7	526.8	126.1	25.3	26.1	73.9
3	1.00	382.1	573.4	191.3	38.3	64.4	35.6
4	0.85	355.4	456.4	101.0	20.2	84.7	15.3
5	0.71	351.1	396.0	44.9	9.0	93.6	6.4
6	0.60	347.7	366.8	19.1	3.8	97.5	2.5
7	0.50	336.5	342.2	5.7	1.1	98.6	1.4
8	0.43	326.0	327.9	1.9	0.4	99.0	1.0
9	0.30	313.1	315.5	2.4	0.5	99.5	0.5
10	Pan	265.8	268.4	2.6	0.5	100.0	0.0
Total				**499.1**	**100.0**	-	-

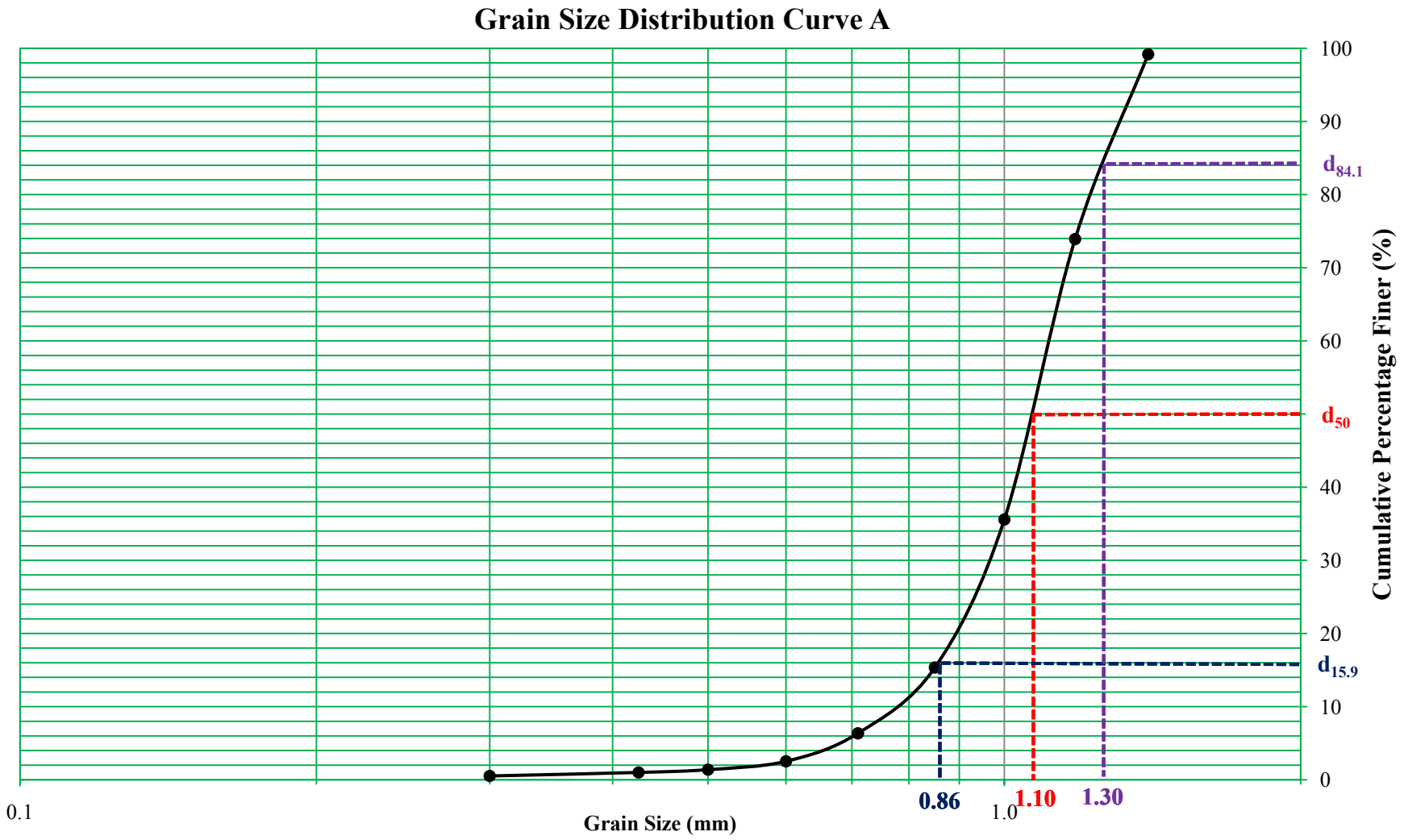

Set B

S/N	Sieve Size (micron)	Empty Sieve Weight (g)	Filled Sieve Weight (g)	Sand Weight (g)	% Retain	% Coarser	% Finer
1	1.40	408.5	413.0	4.5	0.9	0.9	99.1
2	1.18	400.7	521.0	120.3	24.0	24.9	75.1
3	1.00	382.1	579.9	197.8	39.5	64.5	35.5
4	0.85	355.4	471.8	116.4	23.3	87.7	12.3
5	0.71	351.1	390.1	39.0	7.8	95.5	4.5
6	0.60	347.7	362.8	15.1	3.0	98.6	1.4
7	0.50	336.7	340.1	3.4	0.7	99.2	0.8
8	0.43	326.1	327.2	1.1	0.2	99.5	0.5
9	0.30	313.1	314.3	1.2	0.2	99.7	0.3
10	0.00	265.8	267.1	1.3	0.3	100.0	0.0
Total				**500.1**	**100.0**	-	-

Grain Size Distribution Curve B

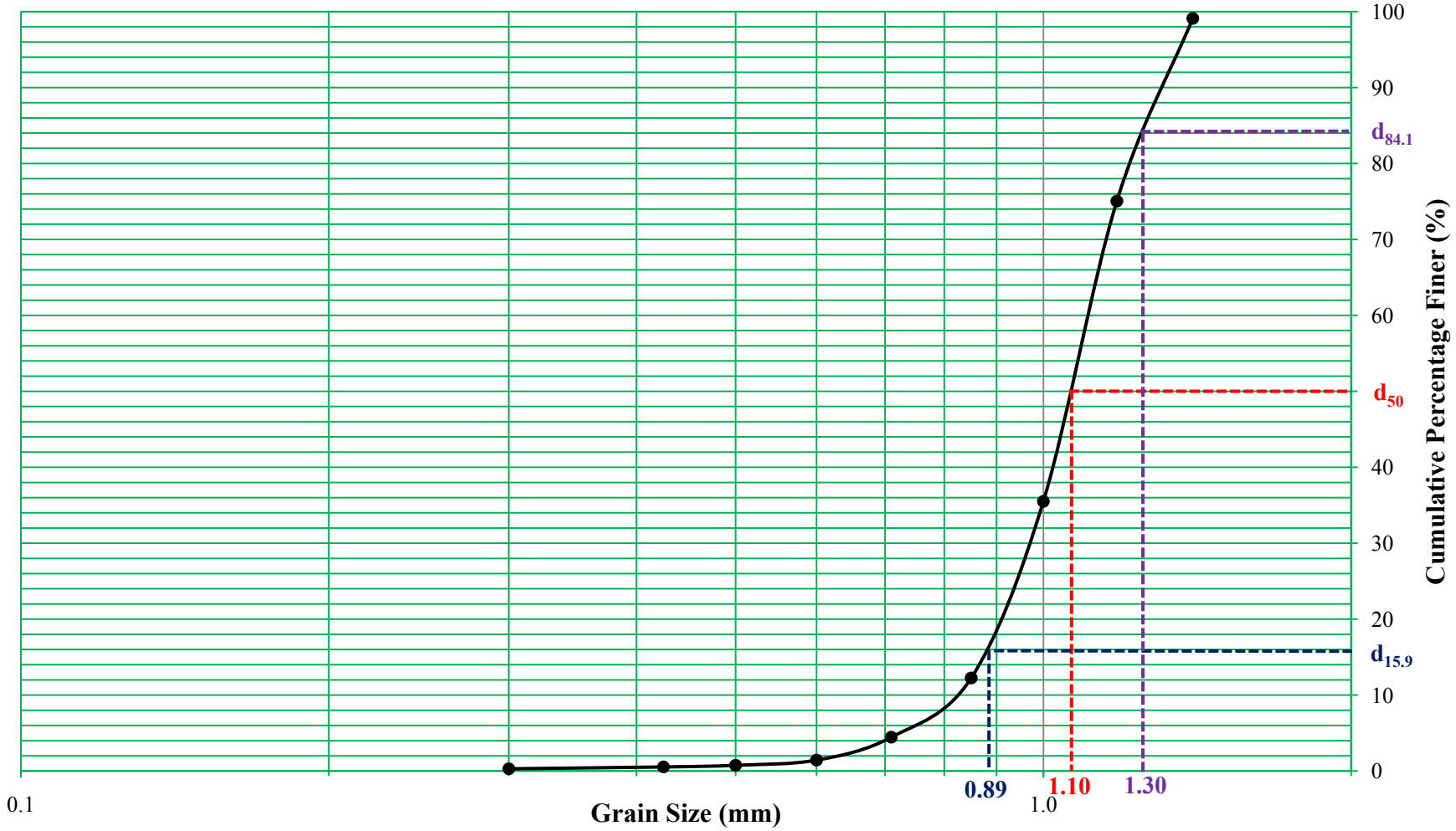

Set C

S/N	Sieve Size (micron)	Empty Sieve Weight (g)	Filled Sieve Weight (g)	Sand Weight (g)	% Retain	% Coarser	% Finer
1	1.40	408.5	414.2	5.7	1.1	1.1	98.9
2	1.18	400.7	488.9	88.2	17.6	18.8	81.2
3	1.00	382.1	563.6	181.5	36.3	55.0	45.0
4	0.85	355.4	481.8	126.4	25.3	80.3	19.7
5	0.71	351.1	409.5	58.4	11.7	92.0	8.0
6	0.60	347.7	372.5	24.8	5.0	96.9	3.1
7	0.50	336.5	345.1	8.6	1.7	98.7	1.3
8	0.43	326.1	328.8	2.7	0.5	99.2	0.8
9	0.30	313.2	315.7	2.5	0.5	99.7	0.3
10	0.00	265.8	267.3	1.5	0.3	100.0	0.0
Total				**500.3**	**100.0**	-	-

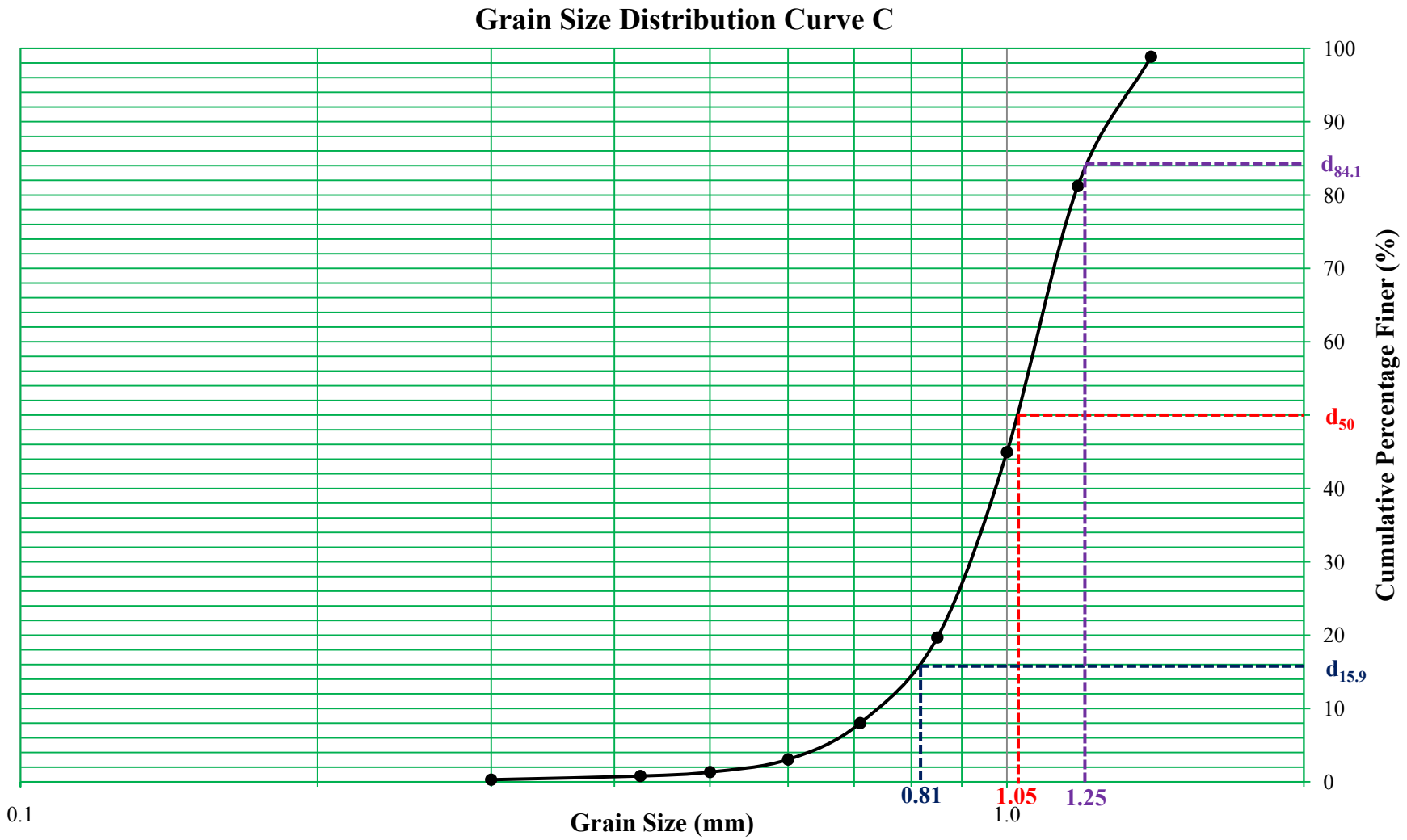

Appendix B Comparison between Measured Flowrate and Computed Weir Discharge

Given that the Discharge Equation *(2-1)*,

$$Q = \frac{2}{3} C_d \sqrt{2g} L_w h^{1.5}$$

Given that the Discharge Coefficient Equation *(2-3)*,

$$C_d = 0.324 \exp\left(0.94 \frac{L_W}{B}\right) \ln\left(1 + \frac{0.73\left(\frac{h}{P}\right) + 3.64}{\exp\left(1.18 \frac{L_W}{B}\right)}\right)$$

Fixed parameters:

- $L_W = 300mm = 0.3m$
- $B = 300mm = 0.3m$
- $L_W/B = 1$ (Suppressed weir)
- $P = 100mm = 0.1m$

$\underline{Measured\ Q\ =\ 1.27L/s}$

$Measured\ h\ =\ 17mm = 0.017m$

$$\frac{h}{P} = \frac{0.017m}{0.100m} = 0.17$$

$$C_d = 0.324 \exp\big(0.94(1)\big) \ln\left(1 + \frac{0.73(0.17) + 3.64}{\exp\big(1.18(1)\big)}\right) = 0.6375$$

$$Computed\ Q = \frac{2}{3}(0.6375)\sqrt{2(9.81m/s^2)}(0.3m)(0.017m)^{1.5} = 0.00125m^3/s = 1.25L/s$$

$\underline{Measured\ Q\ =\ 1.52L/s}$

$Measured\ h\ =\ 19mm = 0.019m$

$$\frac{h}{P} = \frac{0.019m}{0.100m} = 0.19$$

$$C_d = 0.324 \exp\big(0.94(1)\big) \ln\left(1 + \frac{0.73(0.19) + 3.64}{\exp\big(1.18(1)\big)}\right) = 0.6392$$

$$Computed\ Q = \frac{2}{3}(0.6392)\sqrt{2(9.81m/s^2)}(0.3m)(0.017m)^{1.5} = 0.00148m^3/s = 1.48L/s$$

$\underline{Measured\ Q\ =\ 2.00L/s}$

$Measured\ h\ =\ 23mm = 0.023m$

$$\frac{h}{P} = \frac{0.023m}{0.100m} = 0.23$$

$$C_d = 0.324\exp\big(0.94(1)\big)\ln\left(1 + \frac{0.73(0.23) + 3.64}{\exp\big(1.18(1)\big)}\right) = 0.6426$$

$$Computed\ Q = \frac{2}{3}(0.6426)\sqrt{2(9.81m/s^2)}(0.3m)(0.017m)^{1.5} = 0.00199m^3/s = 1.99L/s$$

The tabulation of measured flowrate and computed weir discharge are shown in the following table:

Measured Flowrate (L/s)	**Computed Weir Discharge (L/s)**	**Deviation (%)**
2.00	1.99	0.50
1.52	1.48	2.63
1.27	1.25	1.57

Appendix C Experiment Log

Run	Duration (hr)	Flowrate, Q (L/s)	Tailwater Depth, h_2 (mm)	Apron Length, x (mm)
T1	100.7	5.77	106	0
T2	53.7	2.78	90	
T3	46.8	2.00	82	
T4	147.3	1.61	58	
W1	48.7	1.27	38	
W2	26.6		58	
W3	48.0		70	
W4	118.9		82	
W5	46.7		90	
W6	124.0	1.52	16	
W7	41.9		38	
W8	142.3		58	
W9	49.3		70	
W10	53.4		82	
W11	46.9	2.00	38	
W12	94.5		58	
W13	46.8		70	
W14	117.2		82	
W15	47.2		90	
V1	48.8	1.67	65	
V2	47.4	1.37	66	
A1	49.1	1.52	70	50
A2	28.1			100
A3	48.0			150
A4	6.1			250
A5	48.0			300
A6	48.1			350
A7	48.0			500

Appendix D Derivation of Dimensionless Terms

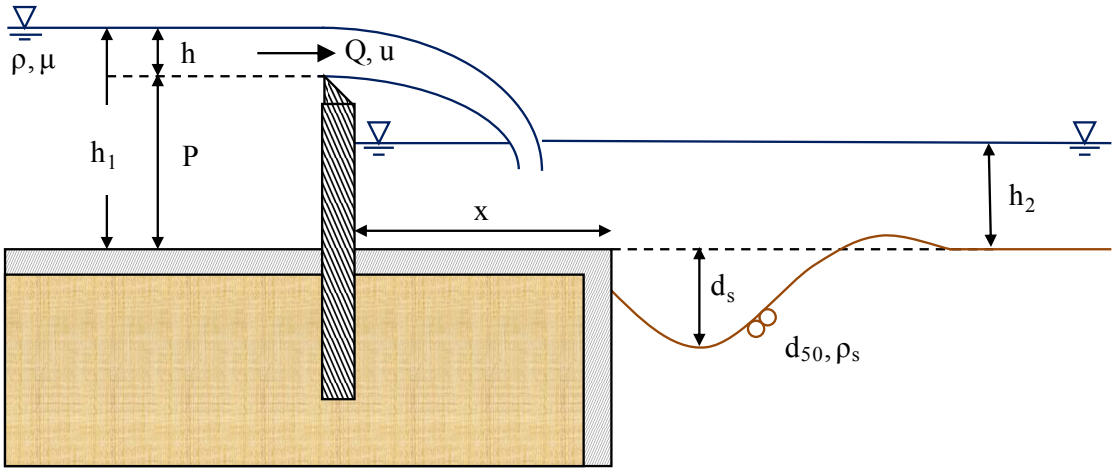

$$(t_e, d_{se}) = f(x, P, h_1, h_2, Q, h, u, g, \mu, \rho, \rho_s, d_{50})$$

Variables	Dimension
Equilibrium Scour Time, t_e	T
Equilibrium Maximum Scour Depth, d_{se}	L
Apron Length, x	L
Weir Height, P	L
Upstream Water Depth, h_1	L
Downstream Water Depth, h_2	L
Flowrate, Q	L^3T^{-1}
Head of Water above Weir Crest, h	L
Average Velocity, u	LT^{-1}
Gravitation Acceleration, g	LT^{-2}
Dynamic Viscosity of Water, μ	$ML^{-1}T^{-1}$
Density of Water, ρ	ML^{-3}
Particle Density, ρ_s	ML^{-3}
Mean Particle Diameter, d_{50}	L

Number of Variables, n = 14

Number of Dimensions, m = 3

Number of π Terms = n – m = 14 – 3 = 11

Repeating Variables: h, g, ρ

Let $\pi_1 = t_e h^a g^b \rho^c = [T][L]^a[LT^{-2}]^b[ML^{-3}]^c$

M: $c = 0$

T: $1 - 2b = 0 \rightarrow b = 0.5$

L: $a + b - 3c = 0 \rightarrow a + 0.5 = 0 \rightarrow a = -0.5$

$\therefore \boldsymbol{\pi_1} = \dfrac{\boldsymbol{t_e g^{0.5}}}{\boldsymbol{h^{0.5}}}$

Let $\pi_2 = d_{se} h^a g^b \rho^c = [L][L]^a[LT^{-2}]^b[ML^{-3}]^c$

M: $c = 0$

T: $-2b = 0 \rightarrow b = 0$

L: $1 + a + b - 3c = 0 \rightarrow 1 + a = 0 \rightarrow a = -1$

$\therefore \boldsymbol{\pi_2} = \dfrac{\boldsymbol{d_{se}}}{\boldsymbol{h}}$

Let $\pi_3 = x h^a g^b \rho^c = [L][L]^a[LT^{-2}]^b[ML^{-3}]^c$

M: $c = 0$

T: $-2b = 0 \rightarrow b = 0$

L: $1 + a + b - 3c = 0 \rightarrow 1 + a = 0 \rightarrow a = -1$

$\therefore \boldsymbol{\pi_3} = \dfrac{\boldsymbol{x}}{\boldsymbol{h}}$

Let $\pi_4 = h_1 h^a g^b \rho^c = [L][L]^a[LT^{-2}]^b[ML^{-3}]^c$

M: $c = 0$

T: $-2b = 0 \rightarrow b = 0$

L: $1 + a + b - 3c = 0 \rightarrow 1 + a = 0 \rightarrow a = -1$

$\therefore \boldsymbol{\pi_4} = \dfrac{\boldsymbol{h_1}}{\boldsymbol{h}}$

Let $\pi_5 = h_2 h^a g^b \rho^c = [L][L]^a[LT^{-2}]^b[ML^{-3}]^c$

M: $c = 0$

T: $-2b = 0 \rightarrow b = 0$

L: $1 + a + b - 3c = 0 \rightarrow 1 + a = 0 \rightarrow a = -1$

$\therefore \boldsymbol{\pi_5} = \dfrac{\boldsymbol{h_2}}{\boldsymbol{h}}$

Let $\pi_6 = Qh^a g^b \rho^c = [L^3T^{-1}][L]^a[LT^{-2}]^b[ML^{-3}]^c$

M: $c = 0$

T: $-1 - 2b = 0 \rightarrow b = -0.5$

L: $3 + a + b - 3c = 0 \rightarrow 3 + a - 0.5 = 0 \rightarrow a = -2.5$

$\therefore \boldsymbol{\pi_6} = \dfrac{\boldsymbol{Q}}{\boldsymbol{g^{0.5}h^{2.5}}}$

Let $\pi_7 = Ph^a g^b \rho^c = [L][L]^a[LT^{-2}]^b[ML^{-3}]^c$

M: $c = 0$

T: $-2b = 0 \rightarrow b = 0$

L: $1 + a + b - 3c = 0 \rightarrow 1 + a = 0 \rightarrow a = -1$

$\therefore \boldsymbol{\pi_7} = \dfrac{\boldsymbol{P}}{\boldsymbol{h}}$

Let $\pi_8 = uh^a g^b \rho^c = [LT^{-1}][L]^a[LT^{-2}]^b[ML^{-3}]^c$

M: $c = 0$

T: $-1 - 2b = 0 \rightarrow b = -0.5$

L: $1 + a + b - 3c = 0 \rightarrow 1 + a - 0.5 = 0 \rightarrow a = -0.5$

$\therefore \boldsymbol{\pi_8} = \dfrac{\boldsymbol{u}}{\sqrt{\boldsymbol{gh}}} = \boldsymbol{Fr}\ (\boldsymbol{Froude\ Number})$

Let $\pi_9 = \mu h^a g^b \rho^c = [ML^{-1}T^{-1}][L]^a[LT^{-2}]^b[ML^{-3}]^c$

M: $1 + c = 0 \rightarrow c = -1$

T: $-1 - 2b = 0 \rightarrow b = -0.5$

L: $-1 + a + b - 3c = 0 \rightarrow -1 + a - 0.5 + 3 = 0 \rightarrow a = -1.5$

$\therefore \boldsymbol{\pi_9} = \dfrac{\boldsymbol{\mu}}{\boldsymbol{h^{1.5}g^{0.5}\rho}} = \dfrac{\boldsymbol{h^{1.5}g^{0.5}\rho}}{\boldsymbol{\mu}}$

Let $\pi_{10} = \rho_s h^a g^b \rho^c = [ML^{-3}][L]^a[LT^{-2}]^b[ML^{-3}]^c$

M: $1 + c = 0 \rightarrow c = -1$

T: $-2b = 0 \rightarrow b = 0$

L: $-3 + a + b - 3c = 0 \rightarrow -3 + a + 3 = 0 \rightarrow a = 0$

$\therefore \boldsymbol{\pi_{10}} = \dfrac{\boldsymbol{\rho_s}}{\boldsymbol{\rho}} = \boldsymbol{S}$

Let $\pi_{11} = d_{50} h^a g^b \rho^c = [L][L]^a [LT^{-2}]^b [ML^{-3}]^c$

M: $c = 0$

T: $-2b = 0 \rightarrow b = 0$

L: $1 + a + b - 3c = 0 \rightarrow 1 + a = 0 \rightarrow a = -1$

$\therefore \boldsymbol{\pi_{11}} = \boldsymbol{\frac{d_{50}}{h}}$

Therefore,

$(\pi_1, \pi_2) = f(\pi_3, \pi_4, \pi_5, \pi_6, \pi_7, \pi_8, \pi_9, \pi_{10}, \pi_{11})$

$$\left(\frac{t_e g^{0.5}}{h^{0.5}}, \frac{d_{se}}{h}\right) = f\left(\frac{x}{h}, \frac{h_1}{h}, \frac{h_2}{h}, \frac{Q}{g^{0.5} h^{2.5}}, \frac{P}{h}, Fr = \frac{u}{\sqrt{gh}}, \frac{h^{1.5} g^{0.5} \rho}{\mu}, S = \frac{\rho_s}{\rho}, \frac{d_{50}}{h}\right)$$

Appendix E Scour-time Development Graphs

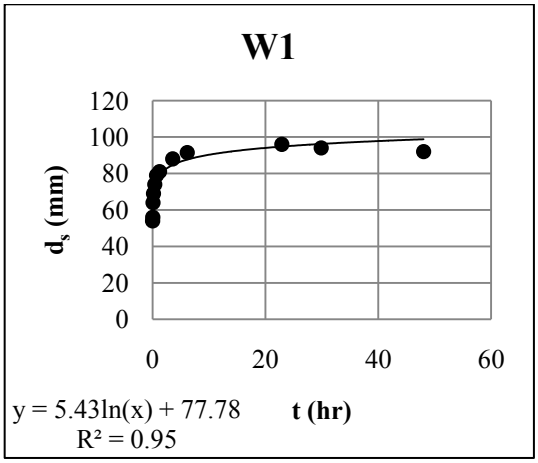

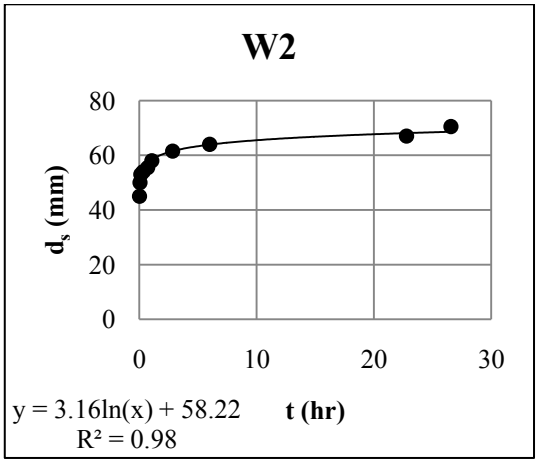

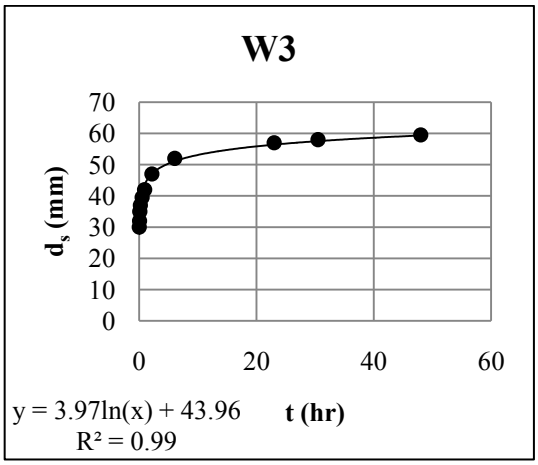

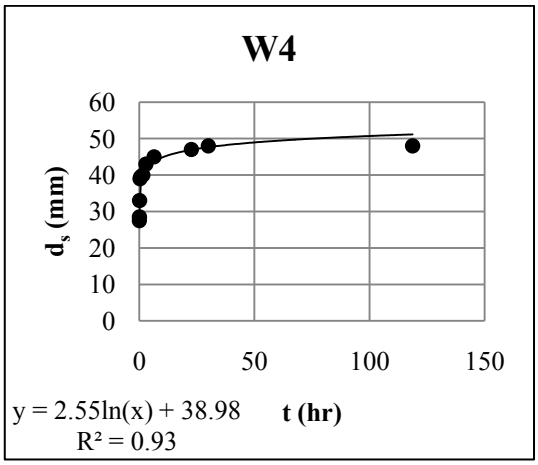

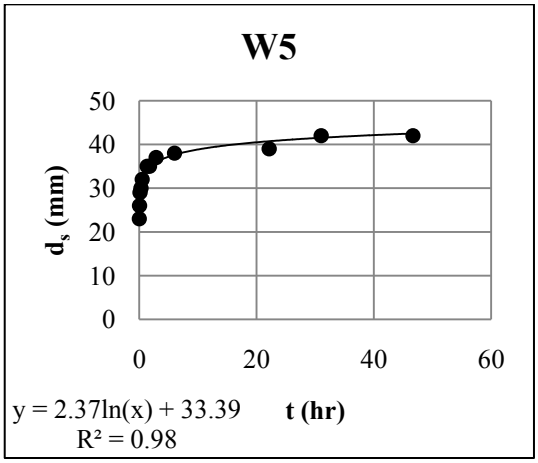

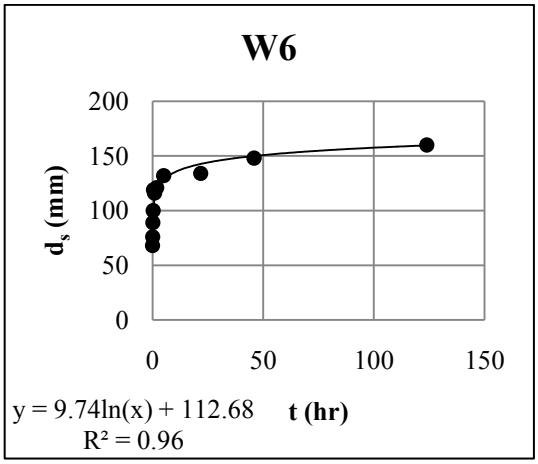

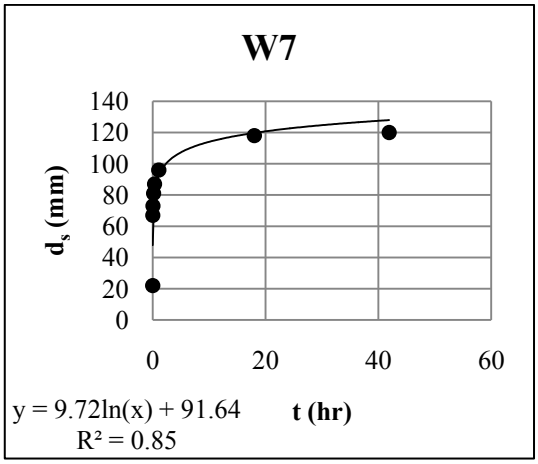

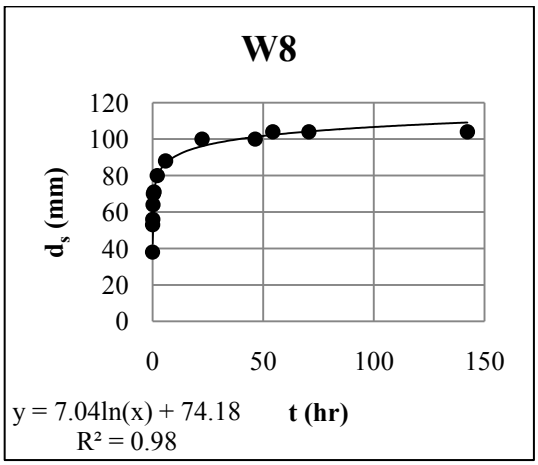

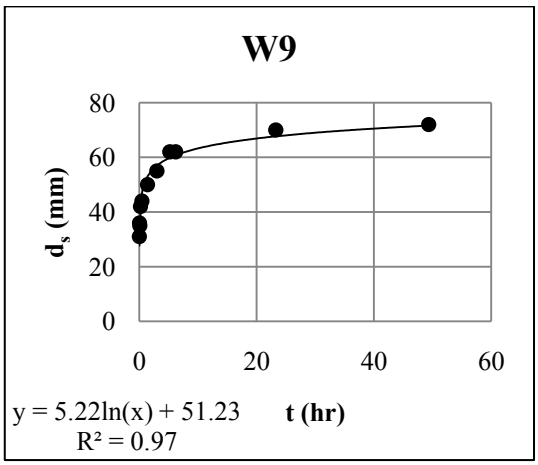

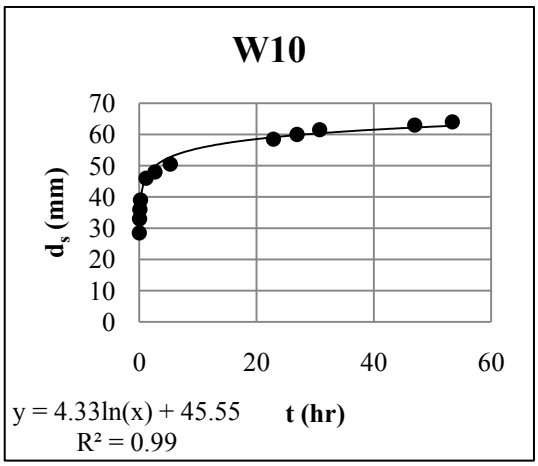

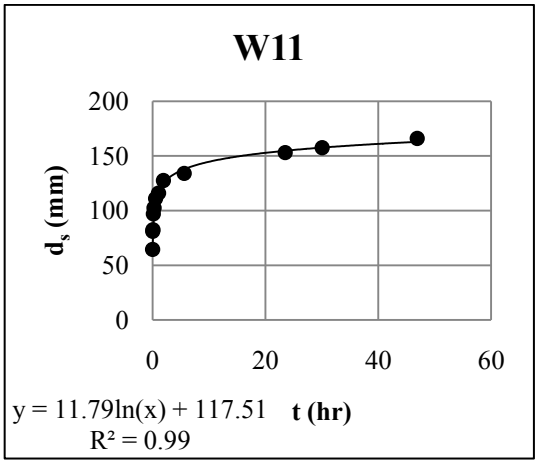

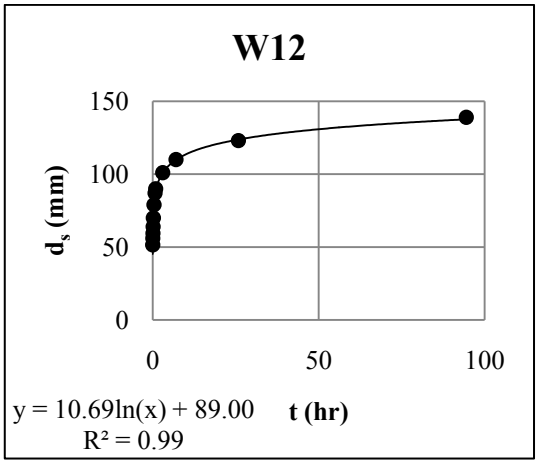

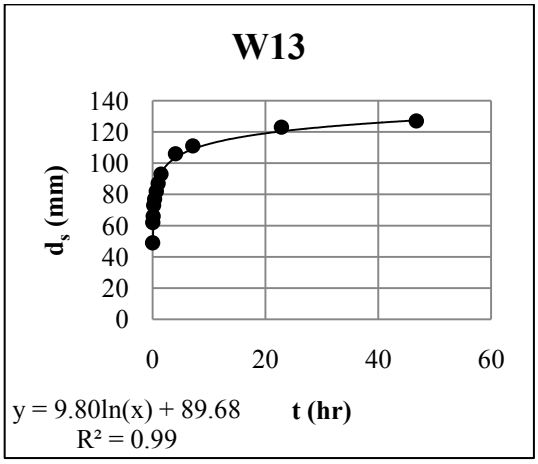

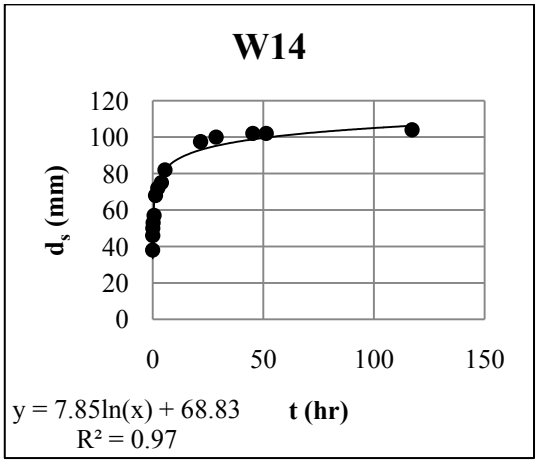

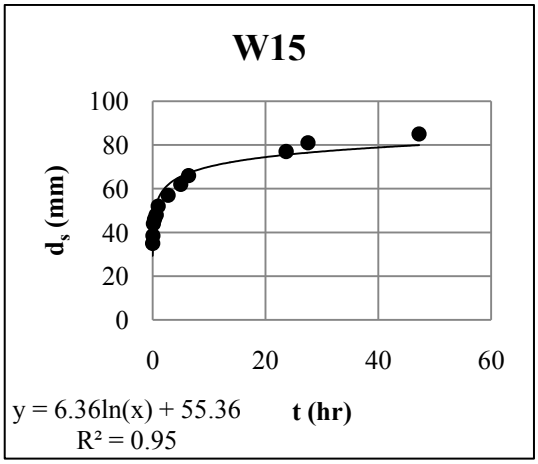

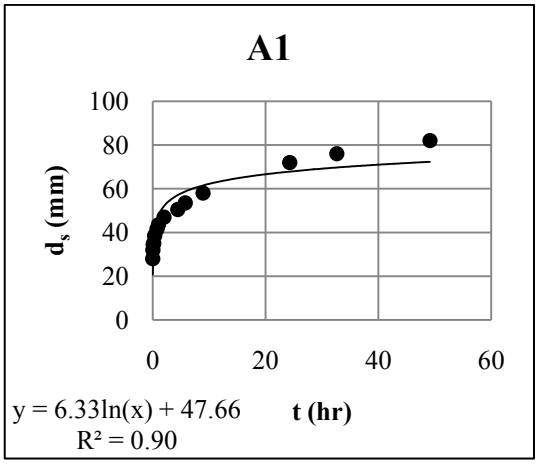

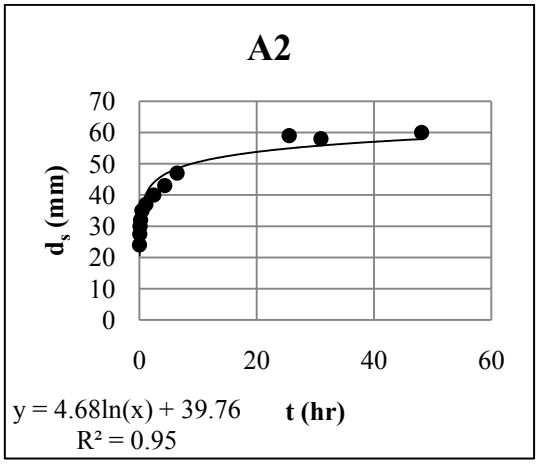

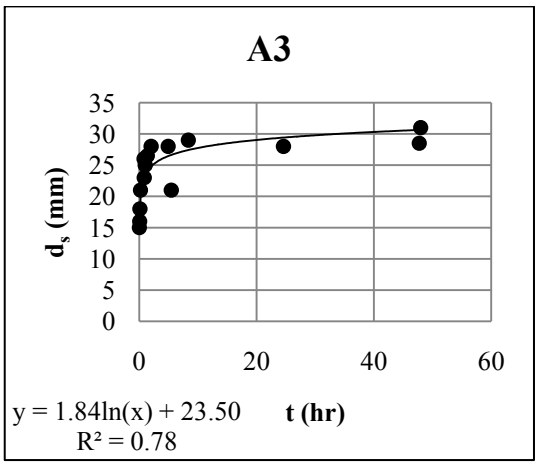

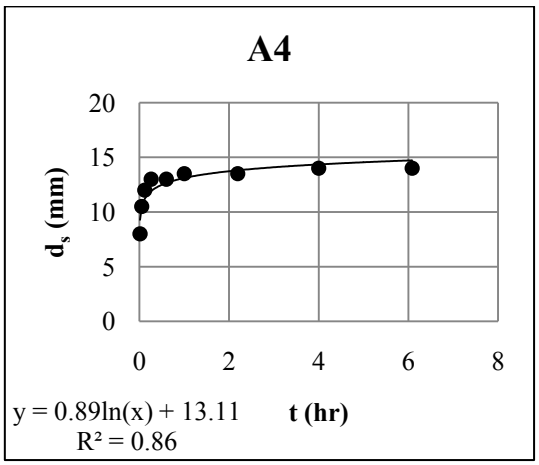

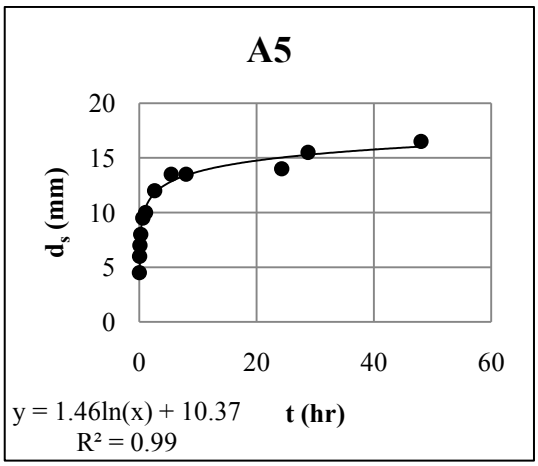

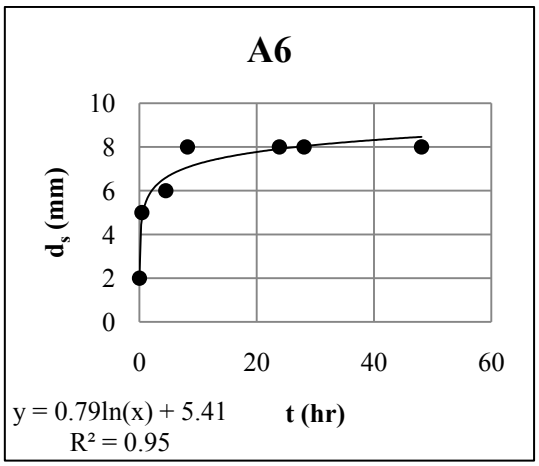

Appendix F Tabulation of Equilibrium Scour Time and Equilibrium Maximum Scour Depth for Runs

Without Apron

Run	Q (L/s)	h_2 (mm)	$d_s(t)$	$d(d_s(t))/dt$	t_e (hr)	d_{se} (mm)	Actual Duration of Run (hr)	d_{sf} (mm)	Deviation (%)
W1	1.27	38	5.43ln(t) + 77.78	5.43/t	27.1	95.7	48.7	89.0	-7.53
W2		58	3.16ln(t) + 58.22	3.16/t	15.8	67.0	26.6	70.5	4.96
W3		70	3.97ln(t) + 43.96	3.97/t	19.9	55.8	48.0	59.5	6.22
W4		82	2.55ln(t) + 38.98	2.55/t	12.7	45.5	118.9	48.0	5.21
W5		90	2.37ln(t) + 33.39	2.37/t	11.8	39.2	46.7	42.0	6.67
W6	1.52	16	9.74ln(t) + 112.68	9.74/t	48.7	150.5	124.0	160.0	5.94
W7		38	9.72ln(t) + 91.64	9.72/t	48.6	129.4	41.9	120.0	-7.83
W8		58	7.04ln(t) + 74.18	7.04/t	35.2	99.3	142.3	104.0	4.52
W9		70	5.22ln(t) + 51.23	5.22/t	26.1	68.3	49.3	72.0	5.14
W10		82	4.33ln(t) + 45.55	4.33/t	21.6	58.9	53.4	64.0	7.97
W11	2.00	38	11.79ln(t) + 117.51	11.79/t	59.0	165.6	46.9	166.0	0.24
W12		58	10.69ln(t) + 89.00	10.69/t	53.5	131.5	94.5	139.0	5.40
W13		70	9.80ln(t) + 89.68	9.80/t	49.0	127.8	46.8	127.0	-0.63
W14		82	7.85ln(t) + 68.83	7.85/t	39.2	97.6	117.2	104.0	6.15
W15		90	6.37ln(t) + 55.36	6.35/t	31.8	77.4	47.2	85.0	8.94
								Average	3.42

Note

d_{sf} denotes the maximum depth of scour hole corresponding the end of experiment

With Apron

Run	Q (L/s)	h_2 (mm)	x (mm)	d_s (t)	$d(d_s(t))/dt$	t_e (hr)	d_{se} (mm)	Actual Duration of Run (hr)	d_{sf} (mm)	Deviation (%)
A1	1.52	70	50	6.33ln(t) + 47.66	6.33/t	31.6	69.5	49.1	82.0	15.24
A2			100	4.68ln(t) + 39.76	4.68/t	23.4	54.5	28.1	60.0	9.17
A3			150	1.84ln(t) + 23.50	1.84/t	9.2	27.6	48.0	31.0	10.97
A4			250	0.89ln(t) + 13.11	0.89/t	4.5	14.4	6.1	14.0	-2.86
A5			300	1.46ln(t) + 10.37	1.46/t	7.3	13.3	48.0	16.5	19.39
A6			350	0.79ln(t) + 5.41	0.79/t	3.9	6.5	48.1	8.0	18.75
A7			500	0	0	0	0	48.0	0	-
									Average	11.78

Note

d_{sf} denotes the maximum depth of scour hole corresponding the end of experiment

Appendix G Regression Analysis

Part 1

Run	Δh/h	Fr_d	$Q/g^{0.5}h^{2.5}$	Measured $t_e g^{0.5}/h^{0.5}$	Measured d_{se}/h	Take LOG				
						Δh/h	Fr_d	$Q/g^{0.5}h^{2.5}$	$t_e g^{0.5}/h^{0.5}$	d_{se}/h
W1	4.647	1.883	10.761	2346618	5.629	0.667	0.275	1.032	6.370	0.750
W2	3.471	1.883	10.761	1367671	3.938	0.540	0.275	1.032	6.136	0.595
W3	2.765	1.883	10.761	1716616	3.284	0.442	0.275	1.032	6.235	0.516
W4	2.059	1.883	10.761	1101747	2.674	0.314	0.275	1.032	6.042	0.427
W5	1.588	1.883	10.761	1024348	2.309	0.201	0.275	1.032	6.010	0.363
W6	5.421	2.017	9.753	3982905	7.922	0.734	0.305	0.989	6.600	0.899
W7	4.263	2.017	9.753	3973907	6.809	0.630	0.305	0.989	6.599	0.833
W8	3.211	2.017	9.753	2881042	5.225	0.507	0.305	0.989	6.460	0.718
W9	2.579	2.017	9.753	2136650	3.593	0.411	0.305	0.989	6.330	0.556
W10	1.947	2.017	9.753	1770180	3.098	0.289	0.305	0.989	6.248	0.491
W11	2.826	2.192	7.959	3973935	5.719	0.451	0.341	0.901	6.599	0.757
W12	3.696	2.192	7.959	4382853	7.199	0.568	0.341	0.901	6.642	0.857
W13	2.304	2.192	7.959	3644199	5.558	0.363	0.341	0.901	6.562	0.745
W14	1.783	2.192	7.959	2917441	4.245	0.251	0.341	0.901	6.465	0.628
W15	1.435	2.192	7.959	2366146	3.365	0.157	0.341	0.901	6.374	0.527

Performing regression analysis on the LOG-terms,

$$\log\left(\frac{t_e g^{0.5}}{h^{0.5}}\right) = 0.655 + 2.156\log\left(\frac{Q}{g^{0.5}h^{2.5}}\right) + 10.741\log(Fr_d) + 0.753\log\left(\frac{\Delta h}{h}\right)$$

$$\log\left(\frac{d_{se}}{h}\right) = -0.050 - 0.493\log\left(\frac{Q}{g^{0.5}h^{2.5}}\right) + 2.610\log(Fr_d) + 0.860\log\left(\frac{\Delta h}{h}\right)$$

Removing the LOG from the function,

$$\log\left(\frac{t_e g^{0.5}}{h^{0.5}}\right) = \log(10)^{0.655} + \log\left(\frac{Q}{g^{0.5}h^{2.5}}\right)^{2.156} + \log(Fr_d)^{10.741} + \log\left(\frac{\Delta h}{h}\right)^{0.753}$$

$$\log\left(\frac{d_{se}}{h}\right) = \log(10)^{-0.049} + \log\left(\frac{Q}{g^{0.5}h^{2.5}}\right)^{-0.493} + \log(Fr_d)^{2.609} + \log\left(\frac{\Delta h}{h}\right)^{0.859}$$

Thus,

$$\frac{t_e g^{0.5}}{h^{0.5}} = 4.52\left(\frac{Q}{g^{0.5}h^{2.5}}\right)^{2.16}(Fr_d)^{10.74}\left(\frac{\Delta h}{h}\right)^{0.75}$$

$$\frac{d_{se}}{h} = 0.89\left(\frac{Q}{g^{0.5}h^{2.5}}\right)^{-0.49}(Fr_d)^{2.61}\left(\frac{\Delta h}{h}\right)^{0.86}$$

Measured $t_e g^{0.5}/h^{0.5}$	**Computed $t_e g^{0.5}/P^{0.5}$**	**% error**	**Measured d_{se}/h**	**Computed d_{se}/P**	**% error**
2346618	2163502	7.80	5.629	5.397	4.13
1367671	1736779	-26.99	3.938	4.199	-6.61
1716616	1463594	14.74	3.284	3.453	-5.16
1101747	1172367	-6.41	2.674	2.680	-0.20
1024348	964363	5.86	2.309	2.144	7.15
3982905	4100048	-2.94	7.922	7.733	2.39
3973907	3421778	13.89	6.809	6.289	7.63
2881042	2764162	4.06	5.225	4.928	5.67
2136650	2344036	-9.71	3.593	4.082	-13.60
1770180	1897359	-7.18	3.098	3.206	-3.50
3973935	3967965	0.15	5.719	6.069	-6.12
4382853	4855698	-10.79	7.199	7.644	-6.18
3644199	3402969	6.62	5.558	5.092	8.38
2917441	2805094	3.85	4.245	4.083	3.81
2366146	2382311	-0.68	3.365	3.388	-0.70
Average Error		**-0.52**	**Average Error**		**-0.19**

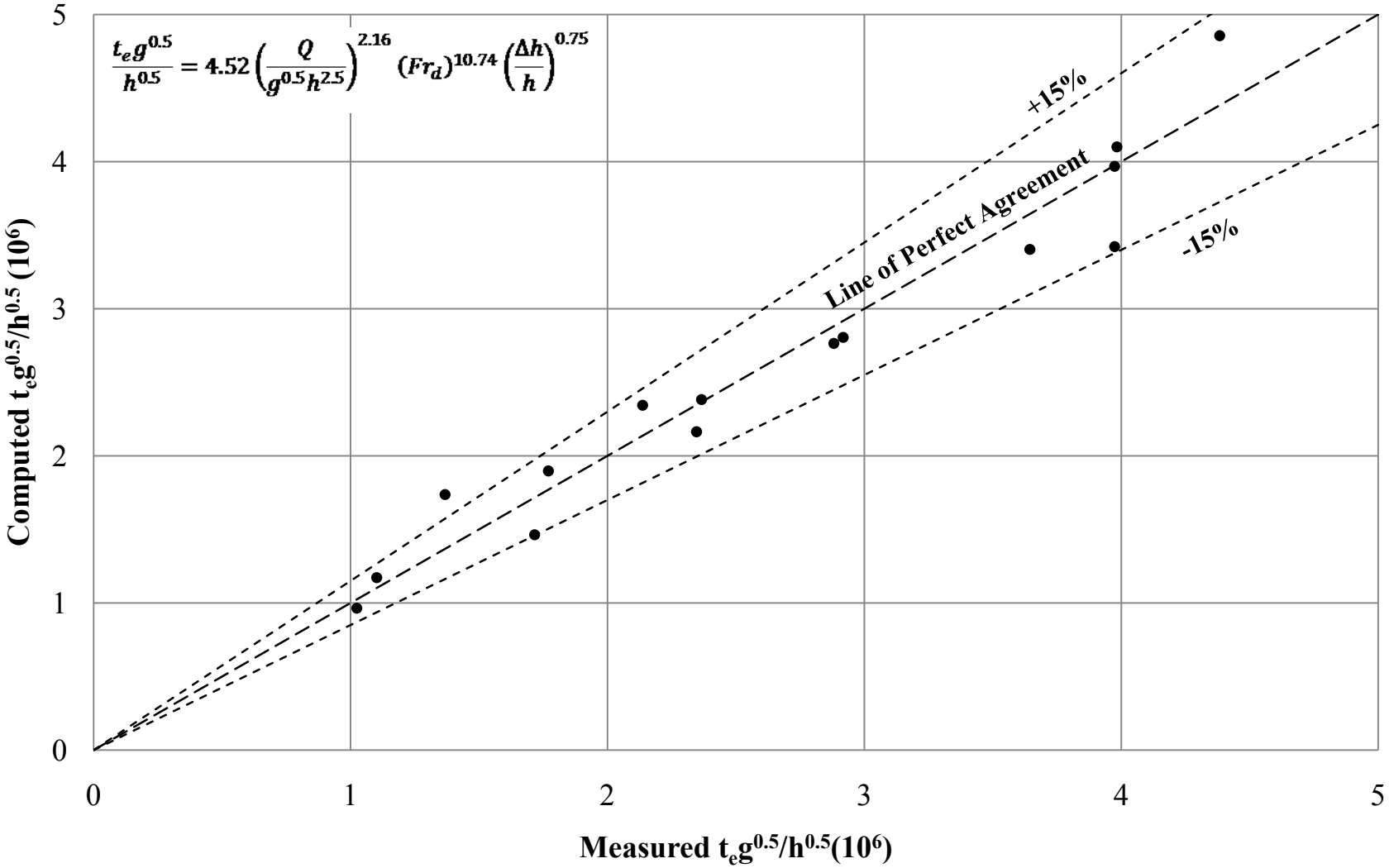

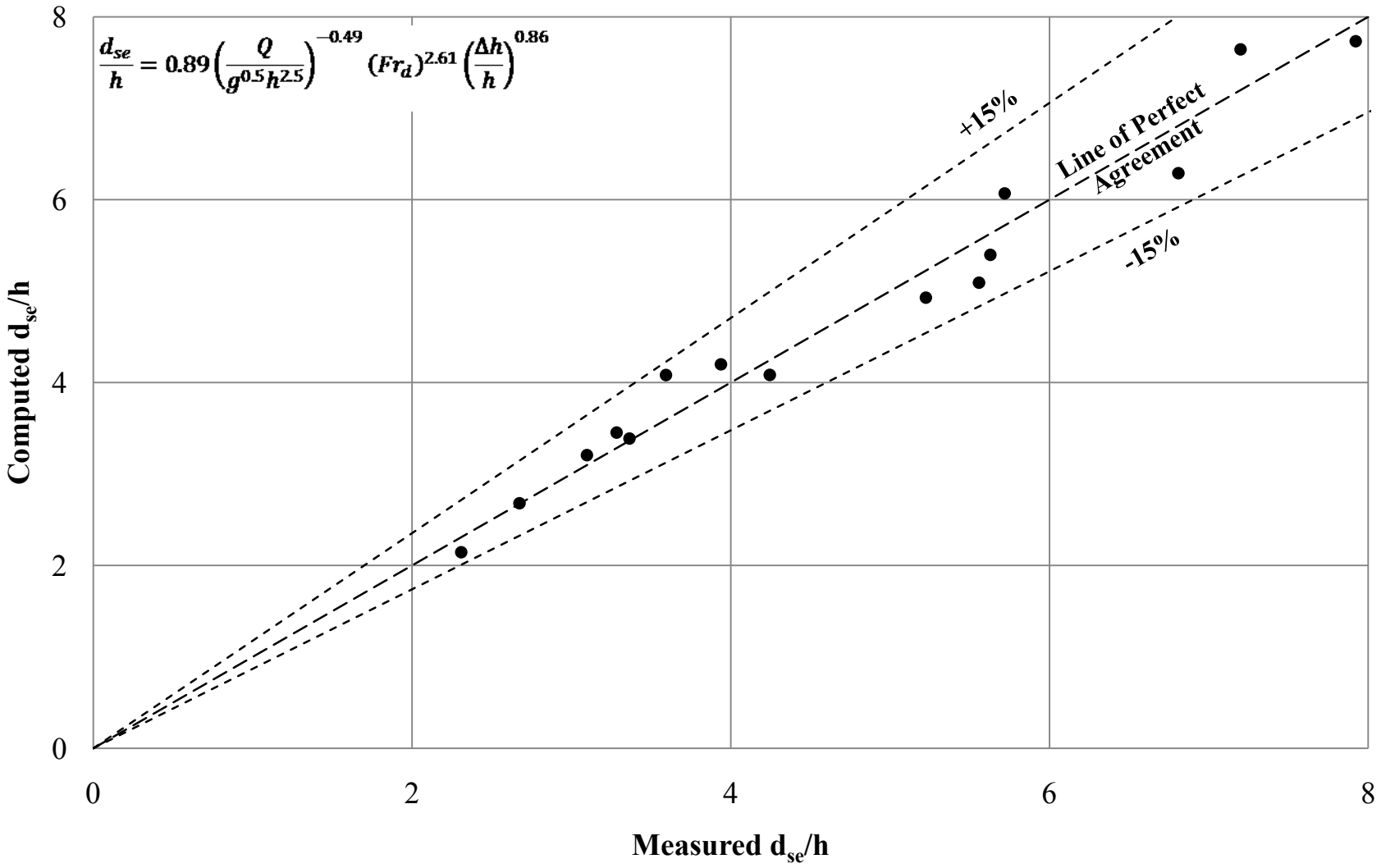

Part 2

Run	Δh/h	Fr	Measured $t_e g^{0.5}/h^{0.5}$	Measured d_{se}/h	Take LOG			
					Δh/h	Fr	$t_e g^{0.5}/h^{0.5}$	d_{se}/h
W1	4.647	1.883	2346618	5.629	0.667	0.275	6.370	0.750
W2	3.471	1.883	1367671	3.938	0.540	0.275	6.136	0.595
W3	2.765	1.883	1716616	3.284	0.442	0.275	6.235	0.516
W4	2.059	1.883	1101747	2.674	0.314	0.275	6.042	0.427
W5	1.588	1.883	1024348	2.309	0.201	0.275	6.010	0.363
W6	5.421	2.017	3982905	7.922	0.734	0.305	6.600	0.899
W7	4.263	2.017	3973907	6.809	0.630	0.305	6.599	0.833
W8	3.211	2.017	2881042	5.225	0.507	0.305	6.460	0.718
W9	2.579	2.017	2136650	3.593	0.411	0.305	6.330	0.556
W10	1.947	2.017	1770180	3.098	0.289	0.305	6.248	0.491
W11	2.826	2.192	3973935	5.719	0.451	0.341	6.599	0.757
W12	3.696	2.192	4382853	7.199	0.568	0.341	6.642	0.857
W13	2.304	2.192	3644199	5.558	0.363	0.341	6.562	0.745
W14	1.783	2.192	2917441	4.245	0.251	0.341	6.465	0.628
W15	1.435	2.192	2366146	3.365	0.157	0.341	6.374	0.527

Performing regression analysis on the LOG-terms,

$$\log\left(\frac{t_e g^{0.5}}{h^{0.5}}\right) = 4.052 + 6.466\log(Fr_d) + 0.785\log\left(\frac{\Delta h}{h}\right)$$

$$\log\left(\frac{d_{se}}{h}\right) = -0.828 + 3.588\log(Fr_d) + 0.852\log\left(\frac{\Delta h}{h}\right)$$

Removing the LOG from the function,

$$\log\left(\frac{t_e g^{0.5}}{h^{0.5}}\right) = \log(10)^{4.052} + \log(Fr_d)^{6.465} + \log\left(\frac{\Delta h}{h}\right)^{0.785}$$

$$\log\left(\frac{d_{se}}{h}\right) = \log(10)^{-0.827} + \log(Fr_d)^{3.588} + \log\left(\frac{\Delta h}{h}\right)^{0.852}$$

Thus,

$$\frac{t_e g^{0.5}}{h^{0.5}} = 11281(Fr_d)^{6.47}\left(\frac{\Delta h}{h}\right)^{0.78}$$

$$\frac{d_{se}}{h} = 0.15(Fr_d)^{3.59}\left(\frac{\Delta h}{h}\right)^{0.85}$$

Measured $t_e g^{0.5}/h^{0.5}$	**Computed $t_e g^{0.5}/P^{0.5}$**	**% error**	**Measured d_{se}/h**	**Computed d_{se}/P**	**% error**
2346618	2261483	3.63	5.629	5.34	5.10
1367671	1797922	-31.46	3.938	4.17	-5.77
1716616	1503722	12.40	3.284	3.43	-4.51
1101747	1192777	-8.26	2.674	2.67	0.19
1024348	972733	5.04	2.309	2.14	7.33
3982905	3974052	0.22	7.922	7.79	1.69
3973907	3290269	17.20	6.809	6.35	6.80
2881042	2633016	8.61	5.225	4.98	4.62
2136650	2216641	-3.74	3.593	4.13	-15.06
1770180	1777582	-0.42	3.098	3.25	-5.06
3973935	4083856	-2.77	5.719	6.03	-5.43
4382853	5042233	-15.04	7.199	7.58	-5.27
3644199	3478702	4.54	5.558	5.07	8.84
2917441	2843180	2.55	4.245	4.07	4.10
2366146	2397315	-1.32	3.365	3.38	-0.55
Average Error		**-0.59**	**Average Error**		**-0.20**

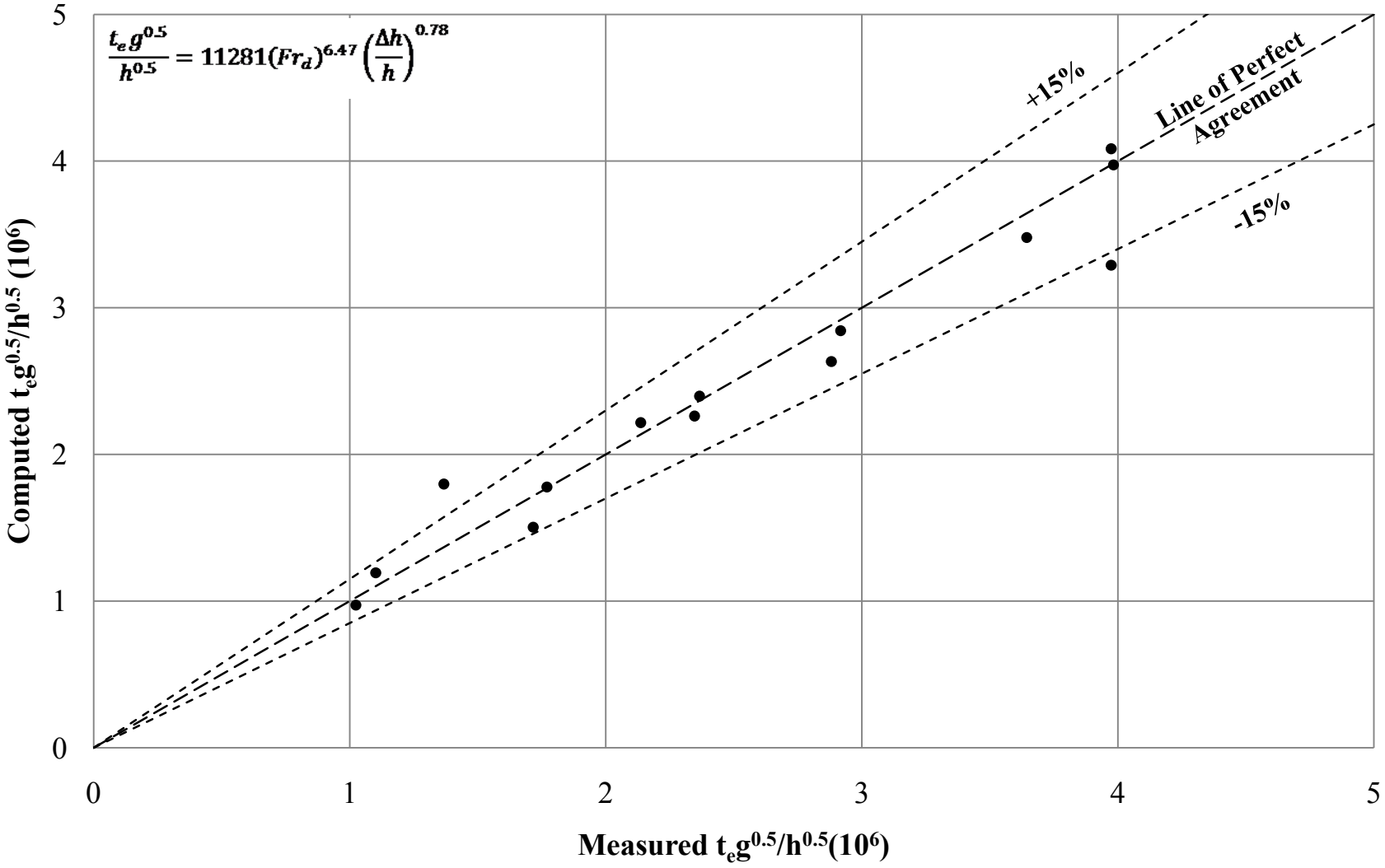

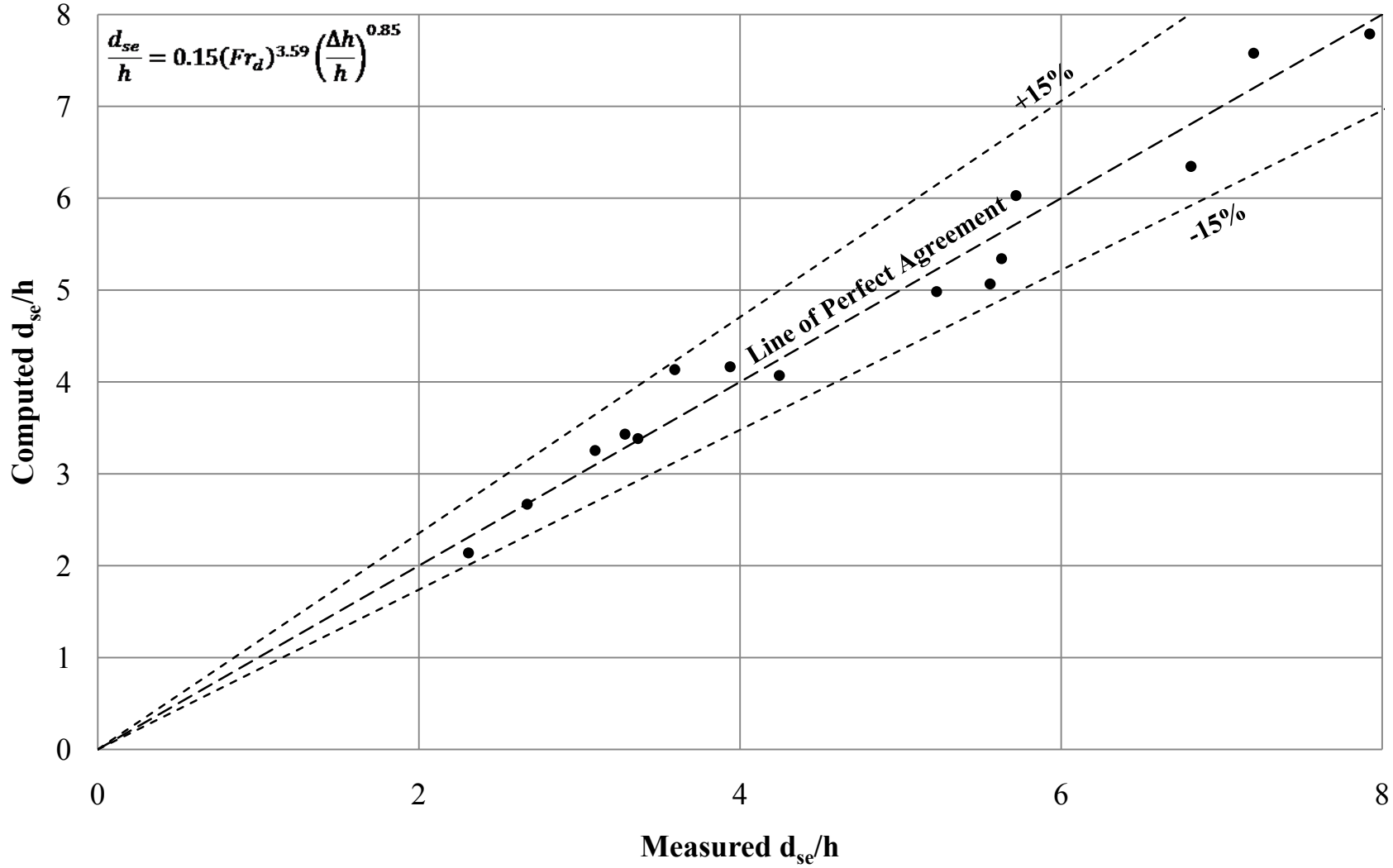

Appendix H Measured and Computed Dimensionless Scour Depth Development